BEHAVIOUR OF IONS IN AN RF PLASMA

Yukio OKAMOTO

Department of Applied Physics
Nagoya University, Nagoya

March 1971

a thesis for DOCTORATE

Abstract

The design and the construction of the electrostatic energy analyzer for low energy of about 10 eV charged particles (resolution is 170), and the quadrupole mass filter with maximum resolving power 100 for 300 eV ions are described.

Accurate energy distributions for each species are obtained. Ion temperature and density ratio of each ion species for steady-state RF plasma are also determined.

The technique described here makes possible to obtain the definitive information about the microscopic properties of plasma: if the energy distribution for ions has no minimum (such as the Maxwellian distribution), there is no instability, while the presence of a deep-enough minimum, such as double-hump in the distribution function, leads to an electrostatic instability. Also, it makes possible a more definitive study of the ion extraction mechanism from the plasma, which is described in detail.

CONTENS

CHAPTER I

Introduction

The study of plasmas generally requires knowledge of the plasma composition (ionic species) and the state of motion of the particles. One wants to know the abundance of ions and their kinetic energy distributions. It is important to know them for understanding the microscopic properties of plasma such as the plasma instabilities and the chemical reactions. The most direct way to get this information is to separate the species and measure the flux of each as a function of particle energy. In the past few years, energy- and mass-analysis for plasma diagnostics has been given by several authors,[1~6] but these measurements were restricted in high energy.

We report here the design and the construction of the apparatus for energy- and mass-analysis which is feasible in the energy region about 10 eV and mass resolving power

of 60, and report also the application for steady-state RF plasma.[7,8] A composition and energy analysis of the ion out-put from the plasma are measured by extracting the ions through a small hole in a metal plane probe and subjecting them to an 90° type electrostatic energy analyzer and a quadrupole mass filter.[7] Great interest in recent years in the mass filter can be explained by several properties which favorably distinguish it from other type of spectrometers:[10,11] in the mass filter, such ion quantities as energy, momentum or velocity are not variables of ion mass separation, in contrast to the majority of static and dynamic spectrometers, which appears to be suitable for the dependence of energy distribution on ionic mass.

The technique described here makes possible to obtain the definitive informations about the microscopic properties of plasma such as the electrostatic instabilities[12,13] and the chemical reactions. It makes also possible to explain the mechanism of ion extraction from a plasma, which is important to determine the energy distribution in the plasma.[8]

The theory of plasma instabilities has been treated extensively during the last two decades, and recently a number of excellent monographs have been written on the subject.[14~18] There exists, however, no comprehensive discussion of the experimental results. This may be partly attributed to the fact that the existing theoretical

analysis are incapable of including the complicated conditions under which plasma instabilities generally occur. This is particularly true in the case of self-excited oscillations, which abound in many plasmas for wave-propagation experiments. Such instabilities are much harder to describe theoretically than externally excited waves.

In the following chapter we shall describe in detail the basic elements of the system, namely, the quadrupole mass filter, the electrostatic energy analyzer and Langmuir probe. In chapter 3, we shall report on energy anomalies of ions effused from an RF plasma, which seem to explain the mechanism of the ion extraction and to determine the ion energies in the plasma. We shall first describe the initial-value problem, then also calculate the spatial dependence of the energy dispersion of ions, since it is of interest in many experimental applications. Finally, the energy distribution function of ions of the plasma will be presented. We shall describe some results not previously published: particle-wave interactions can lead to damping, amplification, and instabilities.

CHAPTER II

Description of Measuring System*

§ 2. 1. Outline of Measuring System

We shall describe the experimental set-up used for the determination of the energy distribution functions with respect to each ion species and collision processes in an RF plasma. A schematic diagram of measuring system is shown in Fig.1. Plasma is produced by an RF power. The positive ions in the plasma effuse (or extract) from a fast-flow system into a high vacuum (5×10^{-7} Torr) through an ion sampling probe with a sampling orifice of 1.0 mm in diameter. This probe is held at a floating (or extracting) potential so that the positive ions

---

* The main part of this chapter was published in Tech. Rep. Inst. Plasma Phys. Nagoya Univ., IPPJ-T-5 (1970).

experience an accelerating field. The ions are directed into a 90° electrostatic energy analyzer and then into a quadrupole mass filter.[7] A Faraday cup or Daly type detector[19] is set at the exit aperture of the mass filter and is connected to a high speed picoammeter and then to an X - Y recorder. Cylindrical Langmuir probes capable of radial displacement are used to determine the radial profile of electron temperature, density, and space (that is, plasma) potential. Low-frequency oscillations are detected by analyzing the frquency spectrum of the ion saturation current. Schematic diagram and photograph of the experimental apparatus are shown in Fig.2.

The following section presents a rather detailed review of quadrupole mass filter, electrostatic energy analyzer and Langmuir probe theory as they are related to the conditions in this experiment.

§ 2. 2. Quadrupole Mass Filter[7]

The instrument used for mass analysis in this work is a quadrupole mass spectrometer originally described by Paul et al..[20,21] The following serves as a brief explanation of how an electrostatic quadrupole field can be used for mass separation.

The electric potential, ϕ_0, which is applied to the poles of the mass filter has the form

$$\phi_0 = U + V\cos\omega t, \qquad (2\text{-}1)$$

where U, V, ω, and t are the dc potential, the peak value of the ac potential, the angular frequency, and time, respectively. The potential for the quadrupole condenser field is

$$\phi(x, y, z, t) = (U + V\cos\omega t)(x^2 - y^2)/r_0^2, \qquad (2\text{-}2)$$

where r_0 is the axis-pole spacing. From this potential we get the equation of motion for a charged particle, viz.,

$$m \frac{d^2x}{dt^2} = - 2e(U + V\cos\omega t) \frac{x}{r_0^2}, \qquad (2\text{-}3)$$

$$m \frac{d^2y}{dt^2} = 2e(U + V\cos\omega t) \frac{y}{r_0^2}, \qquad (2\text{-}4)$$

and

$$m \frac{d^2z}{dt^2} = 0, \qquad (2\text{-}5)$$

where m and e are the mass of the ion and its charge, respectively. Equation (2-5) indicates that the ions move along the z-direction with a constant velocity.

The equations in x and y are identical except for the sign in the second term. If we define $\alpha \equiv \alpha_x = -\alpha_y$ and $\beta \equiv \beta_x = -\beta_y$, where

$$\alpha = \frac{8eU}{mr_0^2\omega^2} \qquad \text{and} \qquad \beta = \frac{4eV}{mr_0^2\omega^2} \qquad (2\text{-}6)$$

then we can write both equations in the canonical form of the Mathieu equation:

$$\frac{d^2u}{d\gamma^2} + (\alpha - 2\beta\cos 2\gamma)u = 0, \qquad (2\text{-}7)$$

where u represents x or y and $\gamma = \omega t/2$. For the x direction we have a direct correspondence between the normal Mathieu equation and the equation of motion. When $\beta = 0$, we have the ordinary harmonic oscillator "α" being the spring constant. The cos term introduces a time dependence of this spring constant and it is obvious that if β is small compared to α, stable oscillations will result, otherwise the time dependent term will dominate and render an unstable solution. For the y direction we have to replace α by $-\alpha$ to obtain the stability diagram. In order that a particle go through the instrument the motion has to be stable in both x and y direction, and the stability diagram for the two directions have to be overlapped. The corresponding Mathieu stability diagram is given in Fig.3. The shaded areas give α- and β-values for stable particle orbits in the quadrupole.

Referring back to the definition of α and β we have (except constant factors and frequency) $\alpha \sim U/m$ and $\beta \sim V/m$; that is, α and β can be adjusted by changing the dc and ac voltage (with frequency ω held constant).

In a practical instrument one operates always in the upper corner of the stability diagram and with a constant ratio $U/V \equiv \lambda$. This corresponds to a straight line in the stability diagram (Fig.3). The value of λ is chosen so that only one mass number gives an α and β pair which is inside the stability region. By varying the magnitudes U and V simultaneously keeping λ constant, one can "push" different masses in the stability region and in this way use the instrument as a mass analyzer. We can change the resolution by varying λ. Lowering λ means that the mass scan line intercepts a wider portion of the stability region and allows stable orbits for more than one mass number. This instrument can be said e/m analyzer since neither the energy (like in the electrostatic analyzer) nor the momentum (which appears in the magnetic analyzer) enters in the equation of motion.

Thus the distinct operating characteristics of this apparatus for the present work are

(1): the operation of the mass filter is independent of the energy dispersion for the ions and their initial velocities, provided that the transit time of an ion inside the dc-ac field is much longer than the period

of the ac field.

(2): the resolving power is easily varied: it has a very high transmission efficiency.

(3): it is capable of operating at considerable residual pressure in the analyzer, allowing the plasma to be sampled at relatively high pressures.

(4): no stray magnetic fields are present that may disturb the plasma.

A mass filter was entirely designed and built in our laboratory as suitable type for studying the electrical discharge. The quadrupole rods are 30 cm in length and 0.8 cm in diameter which are made from stainless-steel. This is operated at a frequency of 2 MHz with a variable voltage for scanning between 1 and 100 amu. The operation of the mass filter requires both a dc and an ac voltage to be applied simultaneously to the quadrupole. The electric circuit is shown in Fig.4. The signals must be 180° out of phase. The components are selected so that the generated voltage ranges from 0 to $\pm$ 850 volts at a frequency 2 MHz. The dc potential proportional to an ac voltage is obtained by diode rectification. The symmetrical variation of the dc potential required by each pair of rods is achieved by an accurately ganged potentiometer. Mass scanning is accomplished by manually varying the screen grid potential of the amplifier. The ac/dc generator is designed so that its frequency is stabilized to better than one part in 10^3.

Through the use of feedback techniques the ac and dc amplitudes are stabilized to better than one part in 10^4. Such a precision are required implicitly by the stability diagram for a satisfactory operation of the mass filter. For the best results also the rods must have an extremely uniform cross-section and must be positioned paralleled to each other with a tolerance of only a few microns.

The resolving power is usually set at a low value of about 1 to 60 in order to (1); minimize the effect of mass discrimination present at high resolution, and (2); maximize the transmission efficiency. A typical spectrum from an air gas discharge is shown in Fig.5. Prominent peaks are obtained at m/e = 14, 16, 28, 30, 32, 40, and 44, presumably corresponding to N^+, O^+, N_2^+ and CO_2^+, NO^+, O_2^+, Ar^+, and N_2O^+ and CO_2^+, respectively. The mean kinetic energy of these ions is 124 eV. More details were reported in ref.7.

§ 2. 3. Electrostatic Energy Analyzer

Hughes et al.[22,23] were the first to demonstrate the particle-focusing properties of cylindrically symmetric, electrostatic potential fields. Later applications appear in the ion or electron energy selector.

If a charged particle moves along the center line of

the analyzer, the equation of motion is given by

$$eE_r = \frac{mv^2}{r_0} , \qquad (2\text{-}8)$$

where e is the electric charge, E_r the radial component of the cylindrically symmetric electric field, r_0 the mean radius of the analyzer, m the ionic mass and v the velocity of ion, respectively. The kinetic energy of the ion can be written by

$$\frac{1}{2} mv^2 = E, \qquad (2\text{-}9)$$

where E is the energy of the ion.

The relation between the analyzer potential V and the energy of the ion is obtained as

$$E = \frac{V}{2 \log r_2/r_1}, \qquad (2\text{-}10)$$

where r_1 and r_2 are the inner- and outer-radius of the deflection plates, respectively. In the present case, r_1 and r_2 are set at 6.7 cm and 7.3 cm, respectively. Equation (2-10) then becomes

$$E = 6.50 \text{ V}. \qquad (2\text{-}11)$$

The resolving power RP of the analyzer with an exit slit width s is given by

$$RP = \frac{E}{\Delta E_i} = \frac{r}{s} , \qquad (2\text{-}12)$$

where ΔE_i is the energy half width (energy dispersion) of the instrumental function, which for a given beam energy is the limit of energy resolution of the analyzer. In the present experiment, s and r are set 0.35 mm and 70.0 mm, so that RP is about 200.

In operating the energy analyzer for low energy charged particles attentions are paid to the following points: (1) to avoid the slitting or broadening of the energy spectrum, metal plate is attached to shield the insulator and (2) to set the slit precisely on the center line of the analyzer electrodes and adjust the slit potential equal to the potential on the center line of the analyzer.

Calibrations for absolute energy and resolving power are done by means of an electron gun. The analyzed beam is collected in a Faraday cup. The incident electron beam at the entrance slit is mono-directional and its intensity is low enough to neglect the space charge effect inside the analyzer. The observed beam energy dispersion of the curve in Fig.6. This, however, is

broader than the actual energy dispersion because of the finite resolving power of the electrostatic analyzer. The apparent energy dispersion ΔE_a can be represented by

$$\Delta E_a^2 = \Delta E_i^2 + \Delta E^2 = \left(\frac{E}{RP}\right)^2 + \Delta E^2 , \qquad (2\text{-}13)$$

where ΔE is the actual energy dispersion and is independent of beam energy. Both the instrumental function and the actual electron energy distribution curve are roughly Maxwellian, and when they are folded together the resultant half width is given by Eq.(2-13). According to the Eq.(2-13), a plot of ΔE_a^2 vs. E^2 should give a straight line having a slope of $(1/RP)^2$ and an intercept equal to ΔE^2. Such a linear plot is shown in Fig.7 for data taken from a series of X-Y traces of the electron energy distribution curve for various beam energies. From the slope of the line, RP is found to be 172. The agreement is good, in view of the considerable uncertainty in the measured slit dimensions. The value of ΔE obtained by extrapolation is 0.1 eV. Energy dispersion of the electron beam caused by an oxide cathode temperature is of the order of 0.1 eV. Thus, the energy resolving power at least 170 for 10 eV electrons is obtained under these conditions.

§ 2. 4. Langmuir Probe[24,25]

Cylindrical Langmuir probes (diameter = 0.1 mmϕ, length = 2 mm) are used to determine the electron density, temperature and plasma potential. Figure 8-(A) shows a typical recorder tracing of the voltage-current characteristics with a probe situated near the axis of the plasma column. Figure 8-(B) is a plot of the logarithm of the electron current as a function of probe voltage used in determining the electron temperature. The electron current is deduced from the total probe current by subtracting the ion current obtained by a straight line extrapolation (shown dashed in Fig.8-(A)). In Fig.8-(B) we see a straight line behaviour over almost two decades of electron current. This suggests strongly that the velocity distribution of electrons is close to a Maxwellian distribution. The electron density and the plasma potential are determined from that part of Fig.8-(A) which corresponds to the regime of ion collection. Since the probe radius is much small compared with the ion Larmor radius, theories for ion collection in the absence of a magnetic field should be applicable. Moreover, the probe radius is small compared with the electron Debye length, thereby permitting the use of Langmuir's orbital-motion theory. According to this theory, the

current I and the applied voltage V are related as follows:

$$I = 2erLN\left(\frac{2kT_i}{m_i}\right)^{1/2}\left[1 - \frac{e(V-V_p)}{kT_e}\right]^{1/2} . \qquad (2\text{-}14)$$

Here r and L are the radius and length of the probe, N the ion density, T_i and T_e the ion and electron temperatures, m_i the ion mass, and V_p the plasma potential (measured relative to ground potential). From Eq.(2-14) we see that I^2 should vary linearly with V. The intercept of the straight line at I = 0 yields the plasma potential (with T_e known from Fig.8-(B)), and the slope of the curve gives the density N.

CHAPTER III

Energy Dispersion of Ion Beam*

§ 3. 1. Introduction

The energy dispersion (spread) of ions effused (or extracted) from an RF plasma is distributed over a range one order of magnitude greater than would result from thermal ion energies in the plasma or from the effect of RF fields acting directly on the ions.[8,26~33] The observed values of the mean beam energy, also, is higher than the applied ion extraction potential.[8,26~33] Such phenomena seem to be an important clue in understanding

---

* The main part of this chapter was published in J. Phys. Soc. Japan, 27 (1969) 270, ibid., 28 (1970) 269, and ibid., 29 (1970) 187, Oyo-Butsuri, 38 (1969) 1114 and Res. Rep. Inst. Plasma Phys. Nagoya Univ. IPPJ-87 (1970).

the mechanism of the sheath formation and the ion beam extraction and in determining the ion energies in the plasma.

While the ion beams extracted from the plasma have been used with positive accelerators and-or isotope separators,[34,35] some have been very successfully employed in scattering experiments and chemical reaction studies.[36,37] For the latter two of these applications it is desirable to have as small dispersion in energy as possible, since low energy beams are usually employed. In this chapter this situation is studied in detail.

§ 3. 2. Experimental Procedure

The experimental equipment used is shown schematically in Fig.9. An RF gas discharge is driven by RF generators (10 ~ 100 MHz) supplying a maximum power of 50 watts. The discharge tube is 20 cm in length and 6 cm in diameter, and is made from Pyrex tube.

The positive ions in the plasma effuse from a fast-flow system into a high vacuum (5×10^{-7} Torr) through an ion sampling probe with a sampling orifice of 1.0 mm in diameter. Other features of the apparatus have been described in § 2. 1. already.

§ 3. 3. Considerations of Experimental Techniques

In view of the fact that electrons are much more mobile than ions, we see a plasma must have a positive potential with respect to a floating plate of ion sampling probe. Most of this potential would occur across the ionic sheath located near the surface of the probe. Thus the ions collected by the probe are accelerated through the potential. If a small hole is drilled on the probe, the accelerated ions at that point can pass through the hole and be energy- and mass-analyzed.

This ion sampling probe behaves as an electrostatic aperture lens. Consequently, ions having different energies when they effuse from the sheath are focussed on an axial focal line. The ions leaving different points on this line have a various angles of divergence. The angular distribution of the ion energies depend on the shape of the plasma-sheath boundary with respect to the optical axis of the orifice lens. When the sheath thickness is much greater than the orifice diameter, however, the focussing properties of the orifice lens are expected to be small, since the hole subtends a very small solid angle at the plasma-sheath boundary, and accepts only those ions which approach the orifice close to normal incidence.

§ 3. 4. General Behaviour of Ion Energy Spectrum.

Varying the potential of the energy analyzer, the energy spectrum can be obtained as shown in Fig.10. It is evident from the figure that the wall of the sampling probe is covered by an ionic sheath such that the positive ions experience an accelerating field, and the electrons experience a retarding field on effusing through the orifice of the probe. In this case the sheath potential corresponds to the peak value in the ion energy spectrum. The curve gives the differentiated translational energy distributions of the positive ions effused from an RF plasma.

As can be seen in Fig.10, the sheath potential proved to be higher than that is expected from the plane probe theory.[25] So, we give here a physical interpretation for such phenomenon.[8,35] Due to the presence of a certain capacitance between the sampling probe and the plasma and between the RF exciting electrode and the plasma, the plasma potential is fluctuated by RF voltage applied to discharge. These capacitances act as a voltage divider of capacity. The behavior of the sheath in the RF discharge, therefore, can be illustrated by the equivalent circuit as in Fig.11. The fluctuations of sheath potential is seen from Fig.11 to be

$$V = V_{C_1} = \frac{C_2}{C_1 + C_2} V_{RF} \simeq \frac{C_2}{C_1} V_{RF} \propto V_s \quad . \qquad (3\text{-}1)$$

where the capacitances C_1 and C_2 represent the capacitance between the probe and the plasma and between the RF exciting electrode and the plasma, respectively. V_{RF} is the RF voltage applied to discharge. V_s is the dc component of the sheath potential of the RF discharge due to a rectifying action of D_1 between the plasma and the sheath. R_1 is the resistance in the sheath. Therefore, the explanations of the following experimental results of the anomalies about the sheath potential (excess energy); (a) the excess energy increases according to the magnitude of the impressed power of RF oscillator,[28,31] (b) the insertion of the electrical shielding screen decreases the excess energy,[30] (c) the excess energy increases according to the increase of the diameter of discharge tube[29] and (d) the excess energy increases according to the decrease of the discharge pressure[33] are as follows. Phenomenon (a) is the increasing of V_{RF}, (b) is the decreasing of C_2, (c) is the increasing of C_2 and (d) is the decreasing of C_1, respectively.

§ 3. 5. Description of Theory

3. 5. 1. Physical situation

It is necessary to consider a plasma containing an electrode which is driven negative with respect to the plasma. The electron temperature will be of the order of 5 eV, the ion temperature much less. The effect of the applied potential is first to drive electrons away from the electrode, creating a positive ion sheath, and then to act on the ions. Because of the smallness of the mass of the electrons compared with that of the ions a first assumption is that the electron movement occures on a much faster time scale than that of the ions, and providing the rate of change of applied potential is not too fast, movement of the electrons under the applied forces may be considered instantaneous.

At any given instant there will be a transition region at the edge of the plasma in which the electron density is steadily decreasing over a distance of the order of the Debye length. This leads into a region almost entirely devoid of electrons and in which the movement will be dominated by ionic space-charge. In practice the magnitude of applied potential will ensure that the thickness of the ionic sheath will be very much greater than the Debye length. Then, we can define the

boundary between the purely ionic sheath and the plasma, within a distance of the order of the Debye length.

The energy of the ions at the plasma boundary will depend on the dynamic situation: in a steady state they will have a velocity of the order of the Bohm velocity $(kT_e/m)^{1/2}$; in a rapidly changing situation field penetration of the plasma will not have acted for sufficient time for them to acquire this velocity, and a value of $(kT_i/m)^{1/2}$, the thermal velocity, is more appropriate. The minimum value of applied potential of interest is of the order of 100 volts, and with an electron temperature of 5 eV this figure gives $eV_p/kT_e \sim 20$. For ions with their thermal velocity this ratio increases by a factor of ten.

If the applied potential (plasma potential) rises rapidly with respect to time the electrons move back into the plasma leaving an ion sheath of thickness s given by direct application of Poisson's equation to a region of uniform charge density en_e as

$$s = \left(\frac{2\varepsilon_0 V_p}{en_e}\right)^{1/2} . \qquad (3\text{-}2)$$

In terms of the Debye length

$$\lambda_D = \left(\frac{\varepsilon_0 kT}{e^2 n_e}\right)^{1/2} , \qquad (3\text{-}3)$$

($\lambda_D \sim 0.6$ mm at T = 5 eV and $n_e = 10^{10}/cm^3$)

we have

$$\frac{s}{\lambda_D} = \left(\frac{2eV_p}{kT}\right)^{1/2} . \qquad (3\text{-}4)$$

In the worst case at the minimum plasma potential this is of the order of ten.

The electric field in the transition region will be of the order of $kT/e\lambda_D$. The average field strength in the sheath is given by

$$\frac{V_p}{s} = \left(\frac{en_e V_p}{2\varepsilon_0}\right)^{1/2} = \frac{kT}{e\lambda_D}\left(\frac{eV_p}{2kT}\right)^{1/2} . \qquad (3\text{-}5)$$

Hence the average field strength in the ionic sheath is at least several times that in the transition region.

3. 5. 2. Formulation of the problem[8,31)]

In the analysis physical and mathematical assumptions are as follows:

(1) The ion velocity is modulated by a time variation of

the plasma potential,

$$V_p(t) = U + V\cos(\omega t + \phi), \qquad (3\text{-}6)$$

where U, V and ω are the dc component of the plasma potential, the amplitude of the time varying component of the plasma potential and the angular frequency of the RF field which is applied to the discharge, respectively.
(2) The thickness of the ion sheath is not displaced.
(3) In this region the space charge field can be neglected i.e., vacuum.

So that it can be assumed that dc and ac potential applied between parallel plane electrode in the vacuum as illustrated in Fig.12. The instantaneous electric field strength in the gap is

$$E(t) = \frac{V_p(t)}{s} = \frac{1}{s}\{U + V\cos(\omega t + \phi)\}, \qquad (3\text{-}7)$$

where s is the gap length (ion sheath thickness). The equation of motion for an ion is then

$$\frac{d^2z}{dt^2} = -\frac{eU}{ms}\{1 + \alpha\cos(\omega t + \phi)\}, \qquad (3\text{-}8)$$

where e/m is the ratio of charge to mass and the fluctuation $\alpha = V/U$ is the ratio of the peak ac voltage

to the dc voltage, which is smaller than unity. Letting z be the displacement of the ion from the plasma-ion sheath boundary and integrating Eq.(3-8) twice, we obtain the ion velocity and the displacement as follows.

$$\frac{dz}{dt} = \frac{eU}{ms}\left\{t + \frac{\alpha}{\omega}\sin(\omega t + \phi) - \frac{\alpha}{\omega}\sin\phi\right\} + v_0 \qquad (3\text{-}9)$$

and

$$z = \frac{eU}{ms}\left\{\frac{1}{2}t^2 - \frac{\alpha}{\omega^2}\cos(\omega t + \phi) - \frac{\alpha}{\omega^2}\cos\phi - \frac{\alpha}{\omega}t\sin\phi\right\} + v_0 t, \qquad (3\text{-}10)$$

where it is assumed that the ion is emitted at ϕ with initial velocity v_0 and zero initial displacement. The transit time of the ion τ which traverse over the distance s is determined by the following equation.

$$\tau^2 - 2\left(\frac{\alpha}{\omega}\sin\phi - \frac{ms}{eU}v_0\right)\tau - \frac{2ms^2}{eU} = 0 , \qquad (3\text{-}11)$$

where it is assumed that $\omega\tau$ is very large. Therefore the transit time of ion τ (positive value) is given by

$$\tau = \frac{\alpha}{\omega}\sin\phi - \frac{ms}{eU}v_0 + \left\{\left(\frac{\alpha}{\omega}\sin\phi - \frac{ms}{eU}v_0\right)^2 + \frac{2ms^2}{eU}\right\}^{1/2} . \qquad (3\text{-}12)$$

The velocity of the ion across the sheath v is, then, defined by

$$\left.\frac{dz}{dt}\right|_{t=\tau} = \frac{eU}{ms}\{\tau + \frac{\alpha}{\omega}\sin(\omega t + \phi) - \frac{\alpha}{\omega}\sin\phi\} + v_0. \tag{3-13}$$

Substituting Eq.(3-12) into Eq.(3-13) results in

$$v = \frac{eU}{ms}\left[\frac{\alpha}{\omega}\sin(\omega\tau + \phi) + \{(\frac{\alpha}{\omega}\sin\phi - \frac{ms}{eU}v_0)^2 + \frac{2ms^2}{eU}\}^{1/2}\right]. \tag{3-14}$$

Using Eq.(1-14) the final energy of the ion E is expressed by

$$\begin{aligned} E &= \frac{1}{2}mv^2 \\ &\simeq eU + \frac{1}{2m}(\frac{eV}{s\omega}\sin\phi)^2 + \frac{mv_0^2}{2} - \frac{v_0V}{s\omega}\sin\phi \\ &\quad + \frac{e}{2m}\{\frac{V}{d\omega}\sin(\omega\tau + \phi)\}^2 \\ &\quad + (\frac{2eU}{m})^{1/2}\frac{eV}{s\omega}\sin(\omega\tau + \phi)[1 + \frac{1}{2}\{\sqrt{\frac{eU}{2m}}\frac{\alpha}{s\omega}\sin\phi \\ &\quad - \sqrt{\frac{mv_0^2}{2eU}}\}^2] \\ &\simeq eU + \frac{mv_0^2}{2} + \sqrt{\frac{2eU}{m}}\frac{eV}{s\omega}\sin(\omega\tau + \phi). \end{aligned} \tag{3-15}$$

Finally, we obtain the energy dispersion of ion ΔE as follows.

$$\begin{aligned}\Delta E &= E_{max.} - E_{min.} \\ &\simeq \frac{eV}{s\omega}\sqrt{\frac{2eU}{m}}\sin(\omega\tau + \phi)\Big|_{max.-min.} \\ &= \frac{2eV}{\omega s}\sqrt{\frac{2eU}{m}} \qquad (3\text{-}16)\end{aligned}$$

The energy dispersion therefore is inversely proportional to the angular frequency of the RF field, inversely proportional to the square root of the atomic mass and proportional to the amplitude of the time-varying component of the plasma potential.

§ 3.6. Results and Discussions

3.6.1. Dependence on an RF exciting frequency

A study is made for the energy dispersion of the positive ions effused from an RF plasma ΔE as a function of the various RF exciting frequency f as shown in Fig.13. From 10 MHz to 85 MHz, ΔE is almost proportional to 1/f when the plasma source is adjusted for optimum operating conditions. The mean kinetic energy of the ions $\bar{E}$ is 102 eV. The expected relation between ΔE and f, based on the assumptions described in § 3. 5. is $\Delta E \propto 1/f$.

This relationship is also shown in Fig.13. Experimental and theoretical results are in good agreement at constant mean kinetic energy of the effused ions.

3. 6. 2. Dependence on ionic mass[32)]

Ionic mass analysis is made by the quadrupole mass filter. Several distinct operating characteristics of the mass filter make it well suited for the dependence of energy dispersion on ionic mass as described in § 2. 2.

To conduct m/e dependence studies satisfactorily, one must first establish the same discharge condition. As the most convenient method, we use the RF discharge produced in air which is a familiar example of mixed gas. A sample spectrum from an air gas discharge is shown in Fig.5. Scanning point of the mass filter located at the each of these ions, the energy dispersion on ionic mass is accompanied by varying the potential on energy analyzer and measuring the corresponding ion current. The dependence of the energy dispersion on ionic mass is shown in Fig.14. The mean kinetic energy of the ions is 124 eV. These values are expected to be inversely proportional to the square root of the mass from Eq.(3-16). The predicted dependence is also shown in Fig.14. Theoretical and experimental results are in good agreement at constant

mean kinetic energy of the effused ions.

3. 6. 3. Dependence on fluctuation of sheath potential

In Fig.15, we show the dependence of the energy dispersion ΔE for N_2^+ ion on the sheath potential, when the discharge pressure P is varied from 5×10^{-5} to 8×10^{-3} Torr. According to Eqs.(3-1) and (3-16), the energy dispersion is proportional to the excess energy and it is coincident with Fig.15 at low pressure ($P \lesssim 7 \times 10^{-4}$ Torr). Where the mean free path for charge transfer is relatively large, many of N_2^+ ions manage to transverse the sheath with no collision with the ambient gas molecules. Thus the high energy N_2^+ ions are able to reach the probe and ion kinetic energy approaches the full sheath potential. In comparison, however, at higher pressure ($P \gtrsim 3 \times 10^{-3}$ Torr), where the energy of ions is less, and high energy N_2^+ ion groups disappear from the observed energy distribution and the energy dispersion become larger. Further, if collisions occur within the sheath, both the ion composition and the sampling efficiency are heavily influenced.

§ 3. 7. Conclusions

An ion extraction model for plasma-sheath system from an RF plasma and its equivalent circuit are presented. All phenomena about the energy anomalies with this model are qualitatively fully explained.

We also proposed here that the energy dispersion of positive ions effused from an RF plasma, under the assumption that the ion velocity is modulated by a time variation of plasma potential, is inversely proportional to the angular frequency of the RF field, inversely proportional to the square root of the ionic mass and proportional to the amplitude of the time-varying component of the potential, theoretically. Experimental results which support the assumptions are obtained.

From the facts described above we may conclude that the level of plasma turbulence affects definitely on the energy distribution.

CHAPTER IV

Energy Distribution Function of Ions*

§ 4. 1. Introduction

A characteristic feature of a plasma is the existence of a spectrum of collective oscillations or plasma waves.[13~15,38] The frequency and velocity of propagation of these waves are determined by the wave vector and by the gross parameters of the plasma such as density, mean velocity spread, magnetic field, etc., and this situation is a reflection of the fact that all of the particles in the plasma are participate in the plasma oscillations. When one examines the growth (or damping) of the oscillations, however, the role of participation is different.

---

* The main part of this chapter was published in Phys. Lett., 32A (1970) 279, and Plasma Phys., 13 (1971) 71.

Growth (or damping) is determined by the "fine detail" of the particle distribution in phase space, for example, by the derivative of the velocity distribution function; this situation reflects the specific role played by resonance particles (i.e., particles for which the following condition is satisfied: $\omega_{\vec{k}} - \vec{k}\vec{v} = n\omega_c$: n = 0, 1, 2, ---; here $\omega_{\vec{k}}$ and $\vec{k}$ are the frequency and wave vector that characterize the wave, $\vec{v}$ is the particle velocity, and $\omega_c \doteq eB/m$). These particles are capable of exchanging energy with the waves and can thus amplify or damp it. To investigate such phenomena, knowledge of the ion velocity distribution function f(v) is required. In this chapter, f(v) is deduced, and the relations between it and the electrostatic instabilities are described.

§ 4. 2. Experimental Procedure

A schematic diagram and the photograph of the experimental setup are shown in Fig.2. Plasma is produced in electron cyclotron resonance (ECR) condition by Lisitano type coil,[39,40] which consists of a slotted cylinder of 3.0 cm in diameter and 10 cm in length fed through a coaxial input connector with a 0 to 100 watts RF power (CW) at a frequency of 2.45 GHz. The plasma container is a Pyrex glass with a diameter of 10 cm and a length of 30 to 100 cm.

A schematic diagram of the coil is shown in Fig.16.

The coil can be regarded as a slotted microwave antenna folded onto a conducting metal cylinder (stainless-steel) so that the electric field across the slot lies in a plane perpendicular to the coil axis. A conducting cylindrical shield is placed coaxialy over the slotted cylinder to prevent out-ward radial power loss. Then, power can radiate only as TE or TM modes inside the slotted cylinder.[41] One end of the slot is one-quarter wave-length long to isolate from the power feed. The rest of the slot, which is folded onto the coil and feeds the energy to the plasma have the length with a nonintegral number of half-wave-lengths to avoid an impedance mismatch where the power is fed into the coil. Even in absence of plasma the coil is not radiating, the diameter being smaller than the cut-off of the wave-length used. Owing to a careful design of a coaxial transition to the input gap of the slotted line, no impedance matching device is necessary. In absence of the plasma the reflected power is large, because the transmission line, slotted over the interior tube of the coil, is shortcircuited at the end of the line. However, in presence of the plasma an excellent impedance match is obtained. The slotted line is immersed in an axial divergent magnetic field set for electron cyclotron resonance in the line.

The energy distribution function of ions is measured by the 90° electrostatic energy analyzer. To identify the

plasma ions, the quadrupole mass filter is used. The low-frequency oscillations are detected by analyzing the spectrum of the ion saturation current drawn by Langmuir probes. The electron temperature and the electron density are measured by Langmuir probes.

§ 4. 3. Some Features of the Plasma

4. 3. 1. Plasma Striations

We observed the formation of plasma striations in this plasma.[10] At a constant RF power and background pressure, we change the magnetic field slowly, and approach to the ECR condition. Then we put the field corresponding to the exact ECR field B_0. When the position of B_0 is in a region 1 in Fig.16, we observe a single plasma striation along the magnetic field lines (Case 1). The location of it is off the magnetic axis and azimutally near the input point of the RF power. An rms voltmeter with a frequency range 10 Hz to 1 MHz is used in the measurement of the persentage of fluctuation in the ion and electron saturation currents to the probe $\{ (\Delta I/I)_{ion}, (\Delta I/I)_{electron} \}$ and in the floating potential fluctuations $e\Delta\phi/kT_e$ (normalized to the electron energy). The observation at the pressure of 2.5×10^{-5} Torr, these values are 10 %, 8 %, and 0.3 %, respectively.

Further increase of the magnetic field strength, B_0 is in a region 2 in Fig.16, causes multiple striations.

With further increasing of the field strength, B_0 is in region 3 in Fig.16, we obtain a well-developed, i. e. , quiescent plasma. Then rms fluctuations of the plasma, at the pressure of 2.5×10^{-5} Torr, above values are 1.6 %, 1.3 %, and 0.1 %, respectively (Case 2). At higher pressure ($P > \simeq 10^{-4}$ Torr) however, the plasma is noisy (Case 3).

We find that transitions between the different number of striations are very sudden. Since we can change the number of striations at a constant RF power and pressure, the observed striations can not simply be related to the coil, which has 12 slots in this experiment. It is more conceivable that different modes are preferentially excited by the coil as the plasma temperature and density change. As we change the magnetic field strength, the rate of power transfer changes. Thus, the temperature and density of plasma can be changed with the magnetic field strength. At the same time, because of the strong interaction between waves and the plasma through heavy damping and the considerable change in medium characteristics, the RF field excited by the coil changes modes with different magnetic field strength.

4. 3. 2. Electron Temperature and Density

Langmuir probes are used to measure the electron temperature and electron density. The plasma properties are

measured as a function of position and the externally controlled plasma conditions, such as RF power, pressure, and magnetic field.

The probes consist of a tungsten wire, of 0.1 mm diameter, insulated by a drawn-down quartz tube, except for an exposed length of 2 mm. The radius of the cylindrical probe is less than the Debye length and much less than the ion Larmor radius, so that the measured probe curves can be interpreted by using the orbital theory of ion collection in the absence of a magnetic field. Details of the data analysis are given in Section 2-4.

Figure 17 shows the electron temperature and the electron density as a function of hydrogen pressure. Figure 18 shows the radial profiles of ion saturation current and floating potential for various flow rate. The average temperature decreases with increasing flow, while the electron density increases substantially as the flow increase. The profile appears to be radially limited by the coil inner radius (1.5 cm). Electron temperature varies from 3 eV to 25 eV, and electron density from 3×10^{8} to 6×10^{10} cm^{-3}, depending on the coupled RF power and the pressure. Experiments are carried out in H_2, He, N_2, and Ar gases.

Two different kinds of low-frequency density fluctuations are observed: the first dominant one lies between 10 to 100 kHz at the Case 1, and with a maximum of wave amplitude in the central region of the plasma column,[11] and the

second dominant one lies between 1 to 15 kHz at the Case 3. It is localized with a maximum wave amplitude mainly at the boundary of the plasma column. The first wave presents a frequency dependence on the ion mass and on temperature which is characteristic of electrostatic sound waves, which will be described in detail in the next Section.[11] The behaviour of the second kind of waves is peculiar one of the drift waves,[42] which will be described in an Appendix A-1.[43]

4. 3. 3. Plasma Composition (ionic species)

The fragmentation pattern of hydrogen is illustrated in the mass spectrum of the observed ions H^+, H_2^+, and H_3^+ are shown in Fig.19. The individual ion densities may be estimated if (1) the singly charged ions detected make up the total ion population in the plasma (H^+, H_2^+, and H_3^+ are the only ions detected with the mass filter), (2) the each ion has an equal ion temperature, and (3) the instrument has an equal over-all sensitivity for each ionic species. The magnitudes of the individual ion currents of the ion sampling characteristics indicate an ion current ratio (Fig.19-(A)), $I_{H^+} : I_{H_2^+} : I_{H_3^+}$ of 1 : 12 : 3.1. The ion density ratio is found from the relation $n_{H^+} : n_{H_2^+} : n_{H_3^+} = (Im^{1/2})_{H^+} : (Im^{1/2})_{H_2^+} : (Im^{1/2})_{H_3^+}$ to be 1 : 17 : 5.7, where m is the mass of the ion.

The composition of the beam of ions extracted from the plasma at low electron temperature is, therefore, mainly molecula. Estimated densities of the charges present in the hydrogen plasma at a pressure of 5×10^{-5} Torr and an electron temperature of 7.1 eV are given in Table 1. Dependence of the individual ion currents on the electron temperature is shown in Fig.20. In general, fragmentation is enhanced at higher ion masses are more aboundant at lower RF power and higher pressures, i.e., at low electron temperature. More detail discussions will be presented in Appendix A-2.[44)]

The observed dependence of the phase velocity on plasma density as will be described in Section 4. 5. 2 can be explained by the fact that H^+, H_2^+, and H_3^+ ions are present in the plasma. In general, for ions of different masses m_1, m_2, m_3, --- with densities n_1, n_2, n_3, --- ($\Sigma n_i = 1$) the phase velocity is given by

$$v_{ph.} \propto (kT)^{1/2}(n_1/m_1 + n_2/m_2 + ---). \quad (4\text{-}1)$$

The variation of frequency with RF power, which at first was not understood, i.e., by increasing the RF power at higher temperature is achieved but the frequency of oscillations is higher than the expected ones from on the temperature, is explained by an increase of the density of H^+ relative to the densities of H_2^+ and H_3^+. Obtaining a reliable information about the microscopic properties of plasma, some knowledge of the plasma composition are, thus, required.

§ 4. 4. Determination of Energy Distribution Function (Maxwellian Distribution Function)

As far as we know, there was no experimental evidence of the existance of the distribution function and temperature for each ion species. We now use a simplified model, and describe the experiments carried out in the quiescent and collisionless RF plasma (case 2). We compare the experimental results with the predictions of the model.

Let us now assume that the ions at the entrance of the ion sampling probe obey the Maxwellian distribution of velocities along a radius in velocity space, and are 'isotropic' within a cone in velocity space of half angle θ_0 (Fig.21). It is also assumed that the velocity distribution is axisymmetric about ϕ, the azimuthal angle in velocity space. This is equivalent to the assumption that the particle motion in the magnetic field is 'adiabatic' in the sense of preserving the magnetic moment of the particle, so that at a particular location of the ion sampling probe with respect to the plasma, the 'escape cone' angle θ_0 is not a function of particle energy. In order to make possible an analytical study, it is assumed that the magnetic field lines, electric field, and analyzer axis are parallel. The source of this plasma is assumed to float at some potential V_p with respect to the grounded zero reference of potential at which analyzer is operated, so that an electric field may exist between the plasma and the analyzer.

The plasma at the analyzer, according to the stated assumptions, will have a distribution function in velocity space given by Loeb,[45]

$$dn(v,\theta,\phi) = \frac{n_0}{\pi^{3/2}} \cdot \frac{v^2}{v_0^3} \exp[-(\frac{v}{v_0})^2] \sin\theta dv d\theta d\phi,$$

$$0 \leq \theta \leq \theta_0 \qquad (4\text{-}2)$$

where v and v_0 are the particle speed and most probable speed m/sec, respectively. n_0 is the particle number density of source particles/m^3. The most probable speed v_0 is given in terms of the kinetic temperature $kT = eV_0$ by

$$v_0 = \sqrt{\frac{2kT}{m}} = \sqrt{\frac{2eV_0}{m}}, \qquad (4\text{-}3)$$

where k is Boltzmann constant, T is kinetic temperature °K, V_0 is the particle kinetic temperature eV, and m is the ionic mass. With the aid of Fig.21, the speed v may be written in terms of the velocity v_z along the analyzer axis,

$$v = v_z \sec\theta. \qquad (4\text{-}4)$$

If Eq.(4-4) is used to change the variable of integration from v to v_z in Eq.(4-2), and an integration over the azimuthal angle $0 \leq \phi \leq 2\pi$ is performed, one obtains,

$$dn(v_z,\theta) = \frac{2n_0 v_z^2}{\pi^{1/2} v_0^3} \exp\left[-\left(\frac{v_z \sec\theta}{v_0}\right)^2\right] \sec^2\theta \tan\theta dv_z d\theta. \quad (4\text{-}5)$$

The differential current density in amperes per square meter of particles impinging on the analyzer is

$$dj(v_z,\theta) = ev\cos\theta dn(v,\theta) = ev_z dn(v_z,\theta) , \quad (4\text{-}6)$$

where j is the current density, A/m^2. Substituting Eq.(4-5) into Eq.(4-6) results in

$$dj(v_z,\theta) = \frac{2n_0 e}{\pi^{1/2}} \left(\frac{v_z}{v_0}\right)^3 \exp\left[-\left(\frac{v_z \sec\theta}{v_0}\right)^2\right] \sec^2\theta \tan\theta dv_z d\theta. \quad (4\text{-}7)$$

Integrating this velocity distribution over the cone in velocity space which contains the particles $0 \leq \theta \leq \theta_0$ yields

$$dj(v_z) = \frac{2n_0 e}{v_0^3 \pi^{1/2}} \int_0^{\theta_0} v_z^3 \exp\left[-\left(\frac{v_z \sec\theta}{v_0}\right)^2\right] \sec^2\theta \tan\theta d\theta dv_z$$

$$= e\frac{n_0 v_z}{\pi^{1/2} v_0} \left[\exp\left\{-\left(\frac{v_z}{v_0}\right)^2\right\} - \exp\left\{-\left(\frac{v_z \sec\theta_0}{v_0}\right)^2\right\}\right] dv_z. \quad (4\text{-}8)$$

When the analyzer is set at some potential $V \geq V_p$, the total transmitted current of positive ions to the collector is given by integrating Eq.(4-8) over the range $v_{z0} \leq v_z \leq \infty$, where

$$v_{z0} \equiv \sqrt{\frac{2e}{m}(V - V_p)} \ , \qquad (4\text{-}9)$$

and therefore the total ion current density is

$$j = \frac{en_0}{2\pi^{1/2}v_0} \int_{v_{z0}}^{\infty} 2v_z [\exp\{-(\frac{v_z}{v_0})^2\} - \exp\{-(\frac{v_z \sec\theta_0}{v_0})^2\}] dv_z . \qquad (4\text{-}10)$$

Performing the integration and substituting Eqs. (4-3) and (4-9), one obtains, for the collector current as a function of analyzer potential,

$$j = \frac{n_0 e v_0}{2\pi^{1/2}} [\exp\{-(\frac{V - V_p}{v_0})\} - \cos^2\theta \exp\{-\frac{(V - V_p)\sec^2\theta_0}{v_0}\}] .$$

$$V \geq V_p \qquad (4\text{-}11)$$

The maximum possible current available to the analyzer occurs when $V = V_p$, because all particles emitted by the plasma are collected. This current is then given by

$$j_{max.} = \frac{n_0 e v_0}{2\pi^{1/2}} \sin^2\theta_0 . \qquad (4\text{-}12)$$

If the velocity distribution of ions in the plasma is , thus, isotropic and Maxwellian with a temperature kT_i, a simple relation is obtained between the energy spectrum measured and the energy distribution of ions in the plasma,

i/e.,

$$\frac{dj}{dE} \propto vf(v)\frac{dv}{dE}v^2 \sin\theta d\theta d\phi \propto E\exp(-\frac{E}{kT_i}), \quad (4\text{-}13)$$

where dj/dE is energy distribution of ion current, which is measured by means of the 90° electrostatic energy analyzer, f(v) is the velocity distribution function in the plasma, $\sin\theta d\theta d\phi$ is solid angle in the velocity space, kT_i is ion temperature in the plasma and $E = e(V - V_p)$ is the thermal energy of ions. The plasma potential V_p is equal to the measured cut-off energy of the spectrum.[46] Figure 22 is a plot of the logarithm of the dj/EdE as a function of ion energy used in determining the ion temperature, which agrees with the energy corresponding to the peak in the spectrum. We also see a straight line over almost one order of magnitude in dj/EdE. These suggest that the velocity distribution of ion is close to a Maxwellian distribution. Figure 23 shows the measured ion temperature as a function of the applied RF power at constant pressure. The ion temperature is, thus, smaller than that of electron.

§ 4. 5. Electrostatic Instability (non-Maxwellian Distribution Function)

4. 5. 1. Introduction

Collective interaction between plasma particles in electrostatic waves is known to Landau growth or Landau damping.[47] In order to understand well such phenomena it is necessary to know the velocity distribution functions of plasma particles. During the last few years this subject has been investigated experimentally with some success.[48~50] Control the distribution functions is more desirable for this purpose. For studying a two-stream ion instability Gabovich et al. produced two-ion beams flowing in the same direction with different velocities.[51,52] Andersen et al. reported to have a double-humped ion velocity distribution function so as to investigate Landau growth of ion acoustic waves.[53]

The existence of ion acoustic waves excited spontaneously or externally, has been discussed by several authors.[54~62] However, the ionic energy distribution function in a plasma has not been examined. In this section, experimental confirmation of the effects of the energy distributions of ions on the ion waves is described. With strongly non-Maxwellian distribution, the ion acoustic wave is excited.[12,13]

One of the problems in fusion research in resent years, while, has been the possible correlation between the presence of finite-amplitude instabilities and anomalous diffusion in the plasma. Most fusion experiments are designed so that the effect of such a correlation is minimized. The usual method of achieving this object is by using complex containing magnetic fields. Another way, however, has been proposed, in which a feedback method is employed in order to stabilize the instability in the plasma system.[63~69] The method essentially relies on being able to detect the presence of an instability and then arranging a feedback of the signal with the correct amplitude and phase such that an external constraint is applied to the plasma in order to damp out the instability. This technique has already been demonstrated fairly successfully on drift instability (Appendix A-1). We report here some experimental results obtain from employing the new method on an ion acoustic instability.[12,13]

4. 5. 2. Results and Discussions[13]

The low-frequency oscillations can be found under the certain conditions. A few typical examples which we observed about the relation between the frequency spectra and the profile of energy distribution functions for the ions are

as follows. When the position of B_0 is in a region 1, as described in Section 4. 3, we observed a single striation in a cold plasma along the magnetic field lines. Then the low-frequency oscillations are excited spontaneously as shown in Fig.24 - (1-a). In this case the energy distribution for the ions is as Fig.24 - (1-b). The distribution function consist of two parts, one is a Maxwellian-like and the other is beam-like uniform higher energy. Increasing of the magnetic field intensity caused multipule striations, and the complicated oscillations and the distributions for ionic energy are observed. When B_0 is in a region 3, no oscillations are observed as shown in Fig.24 - (2-a), and the energy distribution for the ions consists of a single-hump which is a Maxwellian-like distribution as shown in Fig.24 - (2-b). Thus, it can be regarded that the energy distribution function for ions is related to the modes of the plasma and the striations, and the presence of a double-humped distribution function for the ions leads to the instabilities. With the increase in the intensity, we observed the broadening of oscillation spectrum and complex beam-ion energy distribution function. Measurements of the beam distribution function show that the instability is heavily damped at high plasma densities and exhibits a maximum at intermediate densities. These phenomena based

on the magnetic field intensity also have hysteresis.

The observed low-frequency oscillations are interpreted in the following manner; the fixed frequency is assumed to be determined by a standing ionic sound wave, as given by[54)]

$$f = \frac{1}{\lambda}\left\{\frac{\gamma k(T_e + T_i)}{m_i}\right\}^{1/2}, \qquad (4\text{-}14)$$

where f is the observed frequency in cycles per second, λ the wave-length, γ is 3, k is Boltzmann's constant in ergs per °K, T_e and T_i are the electron and ion temperature in °K, and m_i the ionic mass in grams. The wave extends along the plasma column, parallel to the magnetic field. For the fundamental mode of oscillation, the wave-length is twice the length of the plasma column in centimeters. Therefore, for a given length of the plasma column, keeping T_e, T_i, and m_i constant, the wave-length of the self-excited wave should adjust itself to a value depending on the plasma boundary. The measured frequency should then have a dependence on $T = (T_e + T_i)/2$ and m_i as f does. The waves, detected by means of a negatively biased Langmuir probes are coherent, almost sinusoidal. The frequency and amplitude of the ion wave are measured in several lengths of the plasma column L. It is notice-

able that the frequency decreases as the axial wave number (π/L) increases. The predicted dependence of frequency on the length of the plasma column appears to be correct. In Fig.25 the temperature calculated by means of wave frequency measurements versus temperature measured directly by Langmuir probes and the electrostatic energy analyzer (see Sec. 4. 3. 2, and Sec. 4. 4) are plotted for hydrogen, helium, nitrogen, and argon plasma. Good agreement of measured values with calculated ones are obtained, where the compositions of plasma are considered as described in Sec. 4. 3. 3. Thus, the frequency of each system agree with those predicted by the ion acoustic wave formular in terms of temperature, the ion mass and the dimensions of the system. We can conclude, therefore, that the observed low-frequency oscillations in our plasma can be regarded as ion acoustic instability.

The amplitude and the frequency of the ion wave, at a fixed magnetic field, can be controlled by varying the pressure. As the pressure increase the amplitude increase, reaches a maximum and then decrease; at the same time, a certain decrease in oscillation frequency is observed. Figure 26 shows the dependence of amplitude on pressure. The ion wave strongly damped by unionized gas present in the plasma. Gas damping occurs because collisions between

the plasma ions and the gas atoms rob the ions of their coherent ion wave motion. A large energy loss occurs in the collision by two kinds of energy loss effects. The first one is due to the slowing down of ionic energy. The second one is due to the angular deflection of the ions. Only the parallel momentum to the ion wave motion correlate to the sound wave. Thus, the scattering of an ion elastically through a right angle by a much heavier gas atom would not reduce the ion's kinetic energy appreciably, but would deprive the ion sound wave of almost all energy.

In order to suppressed these instabilities, we applied a cusped magnetic field as shown in Fig.27. Increasing the cusped field, 0 to 300 Gauss, the double-humped energy distribution function for the ions changes to the single-humped one, and the instabilities are suppressed gradually. Typical examples which we observed about the relations between the frequency spectra of probe 3 and the profile of the energy distribution function for the ions (1) without- and (2) with-cusped field are shown in Fig.28. As is seen in this figure, there is a strong stabilization effect. It may be noted that in addition to the fundamental frequency ω_1 also the harmonics ω_2 are suppressed. Therefore, it is considered possible that the effect of the ion energy distribution shows decisive influence, the motion of ions

is randomized by the passage of the cusped field, i.e., the plasma beam passes through the field, some of the axial kinetic energy of the particles in the plasma may be changed into the rotational energy, so the energy distribution function changes to a Maxwellian-like distribution.

In sumarry, if the energy distribution function for the ions has no minimum, i.e., single-humped distribution function, such as a Maxwellian distribution, there is no instability, while the presence of a deep-enough minimum, such as double-hump in the distribution function leads to the electrostatic instability. It is important, therefor, the conditions necessary for stability are less restrictive than the sufficient condition: $df(v)/dv < 0$ for all the species.

4. 5. 3. Theoretical Considerations for Data Evaluations

It is well known that a system consisting of a plasma and a beam of charged particles that passes through the plasma can be unstable under certain conditions.[70~75] This is so-called electrostatic instability.

In analyzing the interaction of a beam with the plasma, we shall limit to one-dimensional electrostatic waves. Assume that the ion distribution function has the form shown in Fig.29. The second maximum represents a diffuse beam

of ion superimposed on the main group of thermal ions. As we know, such a velocity distribution is unstable: Langmuir waves with phase velocities in the region where $df(v)/dv > 0$ will increase with time, since the number of ions overtaking a wave and transfering energy to it will be larger than the number of ions withdrawing energy from it. Thus, as a results of Landau's inverse damping mechanism a group of wave will be built up, the phase velocities of which cover the whole interval where $df(v)/dv > 0$.[18)]

If the number of resonance particles is small, i.e., the particle density of the thermal ions, the growth rate of the waves γ will be considerably smaller than the frequency ω. For $\gamma/\omega << 1$, the interaction between the waves can be neglected and we can use the quasi-linear approximation, in which the only non-linear effect considered is the reaction of the oscillations on the "background" the averaged distribution function. The quasi-linear theory can befind the energy loss of the beam and to determine the shape of the spectrum of plasma waves in the system.[18)]

It is, thus, considered possible that the development of the observed instability causes some of the kinetic energyof the striations to be converted into the plasma wave energy.

CHAPTER V

Conclusive Remarks

We conclude the followings:

1). The quadrupole mass filter with maximum resolving power of 100 for 300 eV ions is constructed.

2). The electrostatic energy analyzer for low-energy (> 10 eV) charged particles with resolving power about 170 is constructed.

3). Accurate energy distribution function for each species are obtained with these analyzers.

4). The technique described here makes possible a more definitive study of the ion extraction mechanism from the plasma: the energy dispersion of the ion beam effused from the plasma is inversely proportional to the angular frequency of the RF field, inversely proportional to the root of the ion mass and proportional

to the amplitude of the time-varying component of the plasma potential, respectively.

5). It also makes possible a more definitive information about the microscopic properties of the plasma: the presence of a double-hump in the energy distribution function leads to the electrostatic instability, i.e., particle-wave interactions can lead to instability.

APPENDIX

§ A-1. Drift Waves[42,43]

Drift waves occupy a special place in the spectrum of collective plasma processes. Under laboratory conditions, gradients in temperature, density, magnetic field, and even impurity concentration are inevitable. Wherever a gradient exists, a plasma current or particle drift exists; drift waves are supported by these gradients, and instabilities can tap the energy in the drifts. These phenomena are important at plasma-vacuum and plasma-wall interfaces.

The first drift instabilities were described by Tserkovnikov.[42] He showed that in the presence of temperature gradient in an inhomogeneous plasma, waves propagating exactly across the magnetic field are unstable, and that the phase velocity of these waves is similar to the drift velocity of the particles. Following his work, the stability of high-frequency modes, also propagating exactly across the field, was investigated.[76,77]

Stabilization of drift waves by RF electric fields parallel to the magnetic field have been theoretically predicted both at above the ion plasma frequency and high amplitudes,[68,78] and at frequencies comparable with the frequency of the waves and smaller amplitudes[63] both in collosionless and collisional plasmas. We report here

the results of an experimental investigation on the stabilization of drift waves by an RF electric fields, in a very wide ranges.

The experiments are performed in an RF plasma which is shown in Fig.2. Diagnostics is made by means of radically movable electrostatic Langmuir probes. For detecting the drift wave the probe is biased in the ion saturation current condition. The continuous RF electric field of frequency varying from 300 Hz to 1 MHz, and of amplitude 0 to 20 volts peak to peak, is applied between the Lisitano coil to the ion sampling probe.

In the present Ar plasma, spontaneously excited low-frequency oscillations (1 to 15 kHz) are observed and identified as the drift wave instabilities, after making the important correction for the finite ion inertia and for the plasma rotation due to the radial electric field, which depends on the density and temperature gradients.[79] Radial profiles of ion saturation current (density), floating potential, and the wave amplitudes are shown in Fig.30 (note that wave maxima are localized in the regions of important density and floating potential gradients).

In order to suppresse the wave, we applied an RF electric field. The effects are observed in an appropriate RF frequency and field strength as is seen in Fig.31. At the condition of the drift wave suppression, increasing the RF field strength, the different waves are excited strongly.

Figure 32 shows the stabilizing effects as a function of RF frequency, at the given RF field strength. It is seen that there are two regions where stabilization is effective (suppression of the wave amplitude). One is at frequencies near the frequency of drift wave, and the other is of the ion plasma frequency region, as were observed in Q-machine plasma.[80]

Further results concerning the experimental and theoretical aspects of this work will be published elsewhere.

§ A-2. Chemical Reactions in the Plasma[44]

Although the physical properties of plasmas have received considerable attention, the knowledge of collision processes (in gas discharge it is generally the case that ions in the plasmas suffer the strong coupled collisions with neutral molecules, which lead to ion-molecule reactions) occuring in steady-state plasmas has advanced relatively little. This is the result of the complexities involved in obtaining a representative sample of the ion composition of steady-state discharge. The main purpose, here, is to determine the relative densities of H^+, H_2^+, and H_3^+ ions as a function of electron temperature of the plasma (Fig.20).

Any process important to the formation of atomic ions must compete with the hydrogen molecular ionization process,

$$H_2 + e \rightarrow H_2^+ + 2e. \qquad \text{(A-1)}$$

Because of the distribution of electron energies, the rate at which any reaction proceeds depends on the onset energy and the cross-section immediately beyond onset much more sensitively than on the maximum cross-section. Since reactions

$$H_2 + e \rightarrow H^+ + H + e, \qquad \text{(A-2)}$$

$$H_2 + e \rightarrow 2H^+ + 3e, \qquad \text{(A-3)}$$

may be neglected, the atomic ions must be produced by a two-stage process. Possible processes involve the reactions,

$$H_2^+ + e \rightarrow H^+ + H + e, \qquad \text{(A-4)}$$

$$H_2 + e \rightarrow H + H + e, \qquad \text{(A-5)}$$

and

$$H_2^+ + e \rightarrow H + H. \qquad \text{(A-6)}$$

The number density of molecule ions, however, is much smaller than that of molecules so that the dominant process seems to be reaction (A-5), i.e., dissociation, followed by ionization of the atoms. By way of an example, Fig.33. shows the decomposition levels of the hydrogen molecule. The ion-molecule reaction,

$$H_2^+ + H_2 \rightarrow H_3^+ + H, \qquad \text{(A-7)}$$

may contribute to the production of atomic hydrogen but it is reversible. The most probable process for atomic ion production is, therefore, reaction,

$$H + e \rightarrow H^+ + 2e, \qquad \text{(A-8)}$$

which has a maximum cross-section at an incident electron energy of 40 eV and it is, thus, desirable that the mean electron energy in the plasma should be as close as possible to this value. This feature is almost certainly due to the breaking up a fast molecular ions in collision with gas molecules in the plasma, i.e., at higher electron temperature the collision induced dissociation,

$$H_2^+ + H_2 \rightarrow H^+ + H + H_2, \qquad \text{(A-9)}$$

predominates. However, at lower temperature the ion-molecule reaction,

$$H_2^+ + H_2 \rightarrow H_3^+ + H, \qquad \text{(A-7)}$$

becomes prevalent as is seen in Fig. 20. This reaction is exothermic by about 1.7 eV and is the most probable mode of H_3^+ formation. The tri-atomic molecule H_3 is unstable against dissociation into H_2 and H. Since the formation of the H_3^+ depends on the concentration of both H_2^+ and H_2, the percentage of H_3^+ falls as the percentage of H^+ increase. Use can be made of this to perferentially produce atomic or molecular or tri-atomic ions, respectively.[81] There is

also a great interest in such ion beams as a means of studying chemical reactions.

ACKNOWLEDGEMENTS

I would like to thank my supervisor, Prof. H. Tamagawa, for the guidance and help which he gave me during the course of the work, and for the many hours he spent reading and correcting this thesis.

Thanks are also due to Prof. Y. Miyoshi of Nagoya Institute of Technology for his helpful suggestions and encouragements, and also wish to express their thanks to Prof. K. Takayama, Prof. A. Miyahara, Prof. K. Matsuura, Dr. T. Uchida, and Dr. J. Fujita of Institute of Plasma Physics, Nagoya University for their valuable advices and encouragements.

It is gratefully acknowledged that this work was carried out under the collaborating Research Program at the Institute of Plasma Physics, Nagoya University.

REFERENCES

1). H. P. Eubank and T. D. Wilkerson: Rev. sci. Instrum., 34 (1963) 12.

2). C. R. Erickson: ibid., 37 (1966) 1308.

3). Claude Renaud: EUR-CEA-R 3129.

4). K. W. Ogilive: Rev. sci. Instrum., 39 (1968) 441.

5). R. H. Huddlestone and S. L. Leonard: Plasma Diagnostic Techniques, (Academic Press, New York, 1965) Chap. 12. by J. E. Osker.

6). J. Reece Roth and Marion Clark: Plasma Phys., 11 (1969) 131.

7). Y. Okamoto and H. Tamagawa: Tech. Rep. Inst. Plasma Phys. Nagoya Univ., IPPJ-T-5 (1970).

8). Y. Okamota and H. Tamagawa: J. Phys. Soc. Japan, 29 (1970) 187.

9). W. Paul and H. Steinwedel: Z. Naturforsch, 8a (1953) 448.

10). R. W. Kiser: Introduction to Mass-spectrometry and its Applications (Prentice-Hall Inc., 1965).

11). C. A. McDaniel: Mass-spectrometry (McGraw-Hill, 1963).

12). Y. Okamoto and H. Tamagawa: Phys. Lett., 32A (1970) 279.

13). Y. Okamoto and H. Tamagawa: Plasma Phys., 13 (1971) 71.

14). V. L. Ginzburg: Propagation of Electromagnetic Waves in Plasma (Gordon and Breach, New York, 1961).

15). T. H. Stix: The Theory of Plasma Waves (McGraw-Hill, New York, 1962).

16). Jr. L. Spitzer: Physics of Fully Ionized Gases (Wiley, New York, 1962).

17). J. F. Denisse and J. L. Delcroix: Plasma Waves (Wiley, New York, 1963).

18). M. A. Leontvich: Review of Plasma Physics, vol. 1, 2, 3, and 4 (Consultants Bureau, New York, 1966).

19). N. R. Dalay: Rev. sci. Instrum., 31 (1960) 264 and 720.

20). W. Paul, H. Reinhard and U von Zahn: Z. Physik,152 (1958) 143.

21). Von C . Brunnee, L. Delgmann and K. Kronenberger: Vakuum Technik, 13 (1964) 35.

22). A. Li. Hughes and J. H. Mcmillan: Phys. Rev., 34 (1929) 291.

23). H. Niedermeyer: Inst. Plasma Phys. Munchen, IPP 1/66 (1967).

24). I. Langmuir and H. Mott-Smith: G. E. Review, 27 (1924) 449, 538, 616 and 762.

25). R. H. Huddlestone and S. L. Leonard: Plasma Diagnostic Techniques (Academic Press, New York, 1965) Chap. 4 by F. F. Chen.

26). J. Ero: Nucl. Instrum., 3 (1958) 303.

27). S. M. Levitskii: Soviet Phys. Tech. Phys., 2 (1958) 913.

28). K. J. Cook, O. Heinz, D. C. Lorentz and J. R. Peterson: Rev. sci. Instrum., 33 (1962) 649.

29). T. Tsuchimoto: Japan J. appl. Phys., 5 (1966) 327.

30). J. F. Williams: Rev. sci. Instrum., 37 (1966) 1207.

31). Y. Okamoto and H. Tamagawa: J. Phys. Soc. Japan, 27 (1969) 270.

32). Y. Okamoto and H. Tamagawa: ibid., 28 (1970) 269.

33). Y. Okamoto and H. Tamagawa: Res. Rep. Inst. Plasma Phys. Nagoya Univ., IPPJ-87 (1970).

34). P. C. Thonemann: Nature, 158 (1946) 61.

35). Y. Okamoto and H. Tamagawa: Oyo-Butsuri, (in Japanese) 38 (1969) 1114.

36). E. S. Chambers: UCRL-6987 (1963).

37). D. W. Koopman: Phys. Rev., 154 (1967) 154.

38). B. S. Tanenbaum: Plasma Physics (McGraw-Hill, New York, 1967).

39). G. Lisitano: Proc. 7th, Int. Conf. Ioniz. Phenom. Gases, Beograd, 1 (1966) 464.

40). G. Lisitano, P. Caldirola, N. Barassi, M. Fontanes and E. Sindoni: 3rd Conf. on Plasma Phys. and Cont. Nucl. Fusion Research, Novosibirsk (1968) CN-24/J-4.

41). A. Orefice and R. Pozzoli: J. Appl. Phys., 41 (1970) 3739.

42). V. Tserkonikov: Soviet Phys. JETP 5 (1957) 58.

43). Y. Okamoto and H. Tamagawa: to be submitted in Plasma Phys. (1971).

44). Y. Okamoto and H. Tamagawa: to be submitted in Japan J. appl. Phys., (1971).

45). L. B. Loeb: The Kinetic Theory of Gases (Dover Publication Inc., New York, 1961).

46). C. W. Erickson: Rev. sci. Instrum., 37 (1966) 1308.

47). L. Landau: J. Phys., (USSR), 10 (1946) 45.

48). W. D. Jones and I. Alexeff: Phys. Rev. Lett., 15 (1965) 286.

49). J. H. Malmberg, T. H. Jensen and T. M. O'Neil: 3rd Conf. on Plasma Phys. and Cont. Nucl. Fusion Research, Novosibirsk (1968) CN-24/E-8.

50). H. Böhmer, J. Chang and M. Raether: Plasma Phys., 11 (1969) 645.

51). M. D. Gabovich and G. S. Kirichenko: Soviet Phys., JETP, 23 (1966) 785.

52). T. Honzawa: Phys. Lett., 32A (1970) 335.

53). S. A. Andersen, V. O. Jensen and P. Michelsen: Phys. Lett., 31A (1970) 395.

54). L. Tonks and I. Langmuir: Phys. Rev., 33 (1929) 195.

55). I. Alexeff and R. V. Neidigh: Phys. Rev., 129 (1963) 516.

56). F. W. Crawford and R. J. Kuhler: Proc. Int. Conf. Ioniz. Phenom. Gases, Beograd, 2 (1966) 326.

57). J. H. Malmberg and C. B. Wharton: Phys. Rev. Lett., 19 (1967) 775.

58). C. B. Wharton, J. H. Malmberg and T. M. O'Neil: Phys. Fluids, 11 (1968) 1761.

59). J. H. Malmberg, C. B. Wharton, R. W. Gould and T. M. O'Neil: Phys. Rev. Lett., 20 (1968) 95.

60). J. Musil, F. Žaček, J. Ďatlov and J. Teichmann: Plasma Phys., 11 (1969) 961.

61). G. Lisitano, S. Bernabei and E. Sindoni: Phys. Lett., 29A (1969) 613.

62). G. M. Sessler: Phys. Acoustics, vol.4, part B, Chap.12, Acoustic and Plasma Waves in Ionized Gases (Academic Press Inc., New York, 1968).

63). M. Dobrowolny, F. Engelmann and A. M. Levine: Plasma Phys., 11 (1969) 973 and 983.

64). R. R. Porker and K. I. Thomassen: Phys. Rev. Lett., 22 (1969) 1171.

65). B. E. Keen and R. V. Aldridge: ibid., 22 (1969) 1358.

66). T. C. Simonen, T. K. Chu and H. W. Hendel: ibid., 23 (1969) 568.

67). B. E. Keen: ibid., 24 (1970) 259.

68). Y. Nishida, and M. Tanibayashi and K. Ishii: ibid., 24 (1970) 1001.

69). D. C. Carlyle, E. L. Lindman and M. E. Oakes: Phys. Lett., 33A (1970) 279.

70). V. D. Shapiro: Soviet Phys. JETP, 17 (1963) 416.

71). A. A. Ivanov and L. I. Rudakov: ibid., 24 (1967) 1027.

72). S. M. Levitskii and I. P. Shashurin: Soviet Phys. JETP, 25 (1967) 227.

73). A. A Goncharov and G. S. Kirichenko: Soviet Phys. Tech. Phys., 14 (1970) 1492.

74). W. Herrmann and Th. J. Fessenden: Phys. Rev. Lett., 18 (1967) 535.

75). Ya. B. Fainberg: Int. Symp. on Beam-Plasma Interactions, Prague, IPPCZ-91 (1967).

76). N. A. Krall and M. N. Rosenbluth: Phys. Fluids, 5 (1962) 1435.

77). A. B. Mikhailovskii and A. V. Timofeev: Soviet Phys. JETP, 17 (1963) 626.

78). Ya. B. Fainberg and V. D. Shapiro: ibid., 25 (1967) 187.

79). H. W. Hendel and P. A. Politzer: Proc. of Conf. on Physics of Quiescent Plasmas, Frascati (1967) 181.

80). R. Sciarra, M. Dobrowolny and F. Magistrelli: Phys. Rev. Lett., 25 (1970) 1553.

81). Y. Okamoto and H. Tamagawa: Japan J. appl. Phys., 10 (1971) 165.

Charge Species	Number Density Particles/cc	Percentage Composition
electron	8×10^9	-
total ion	8×10^9	-
H^+	0.34×10^9	4.2 %
H_2^+	5.72×10^9	71.5 %
H_3^+	1.94×10^9	24.3 %

Table 1. Estimated densities of the charged species present in the RF plasma at a pressure of 5.5×10^{-5} Torr and electron temperature of 7.1 eV.

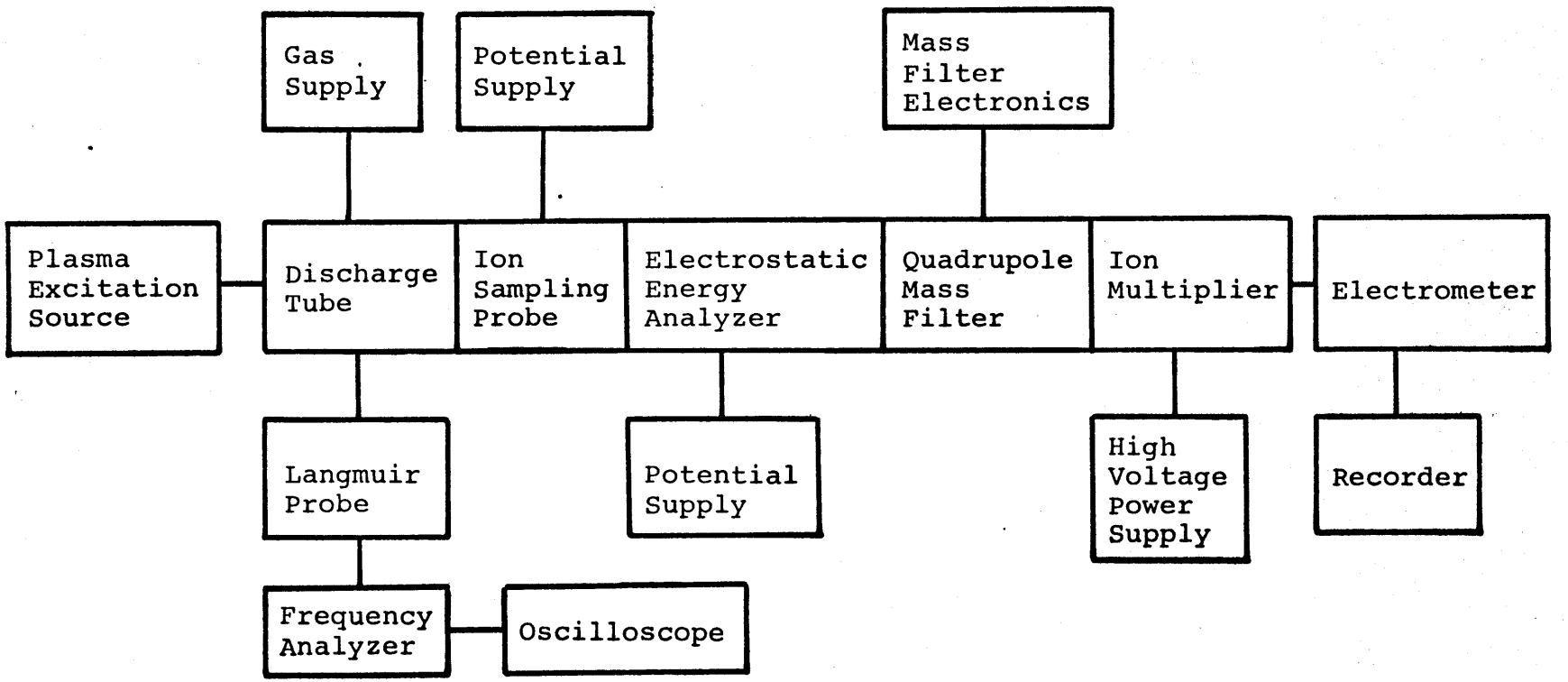

Fig. 1. Block diagram of measuring system.

(A)

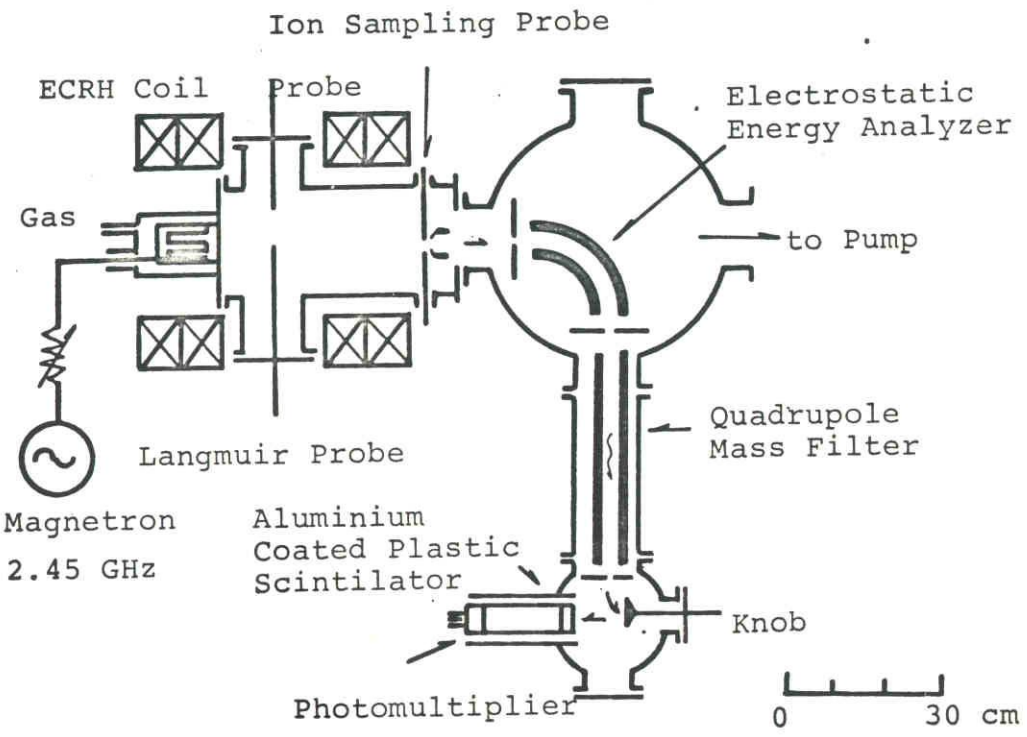

(B)

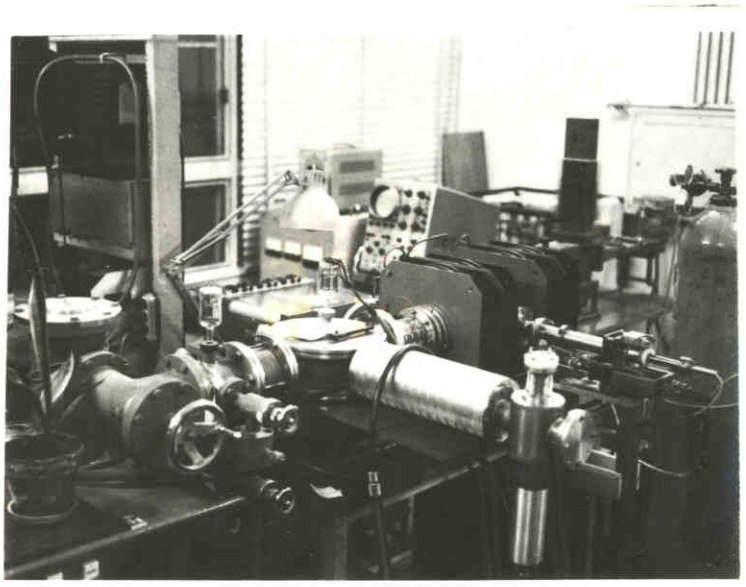

Fig. 2. Schematic diagram (A) and photograph (B) of experimental apparatus.

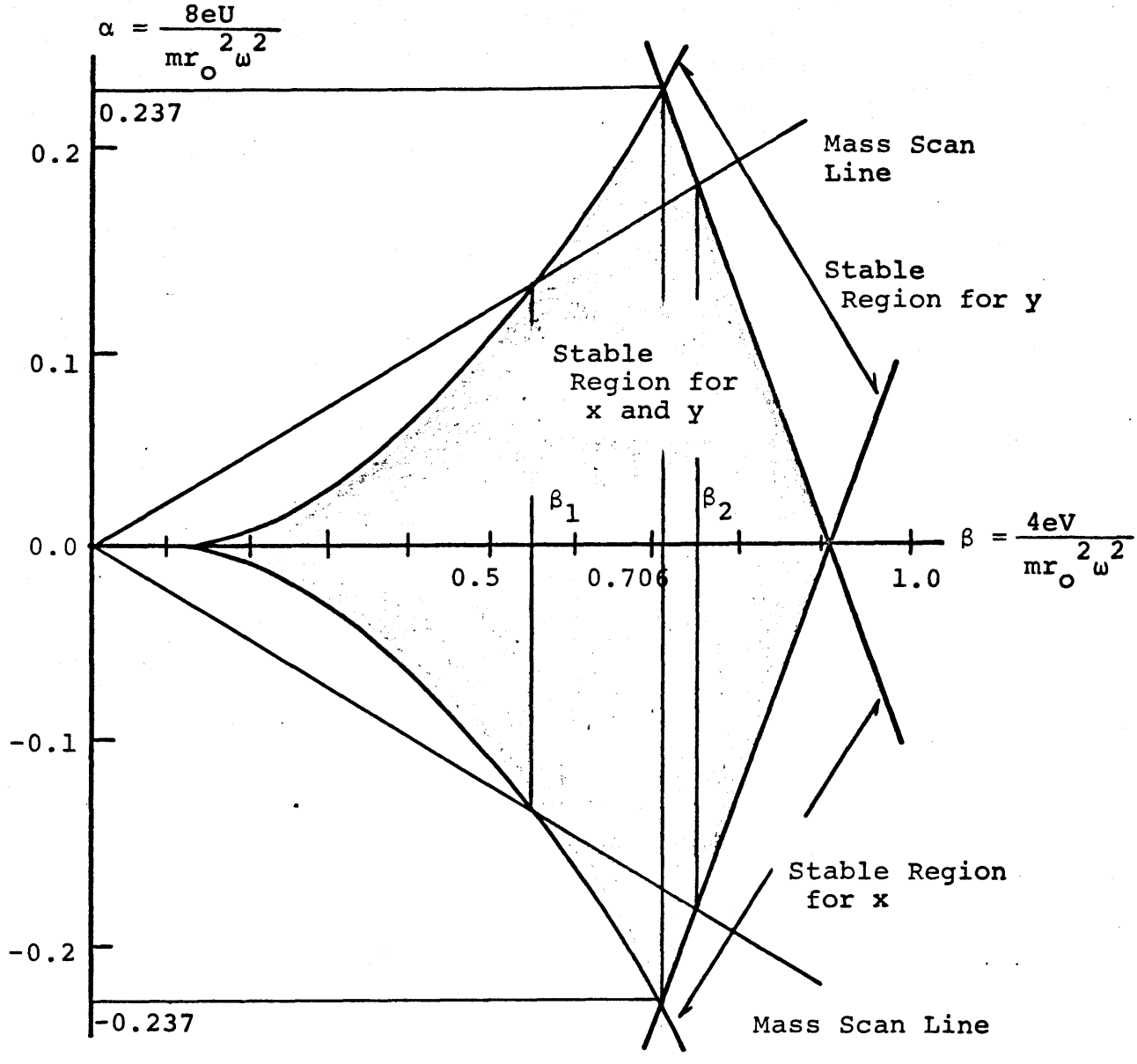

Fig. 3. The corresponding Mathieu stability diagram. Ion transmission in the mass filter occurs for values of the parameters which locate α and β above the scan line and inside the stability diagram.

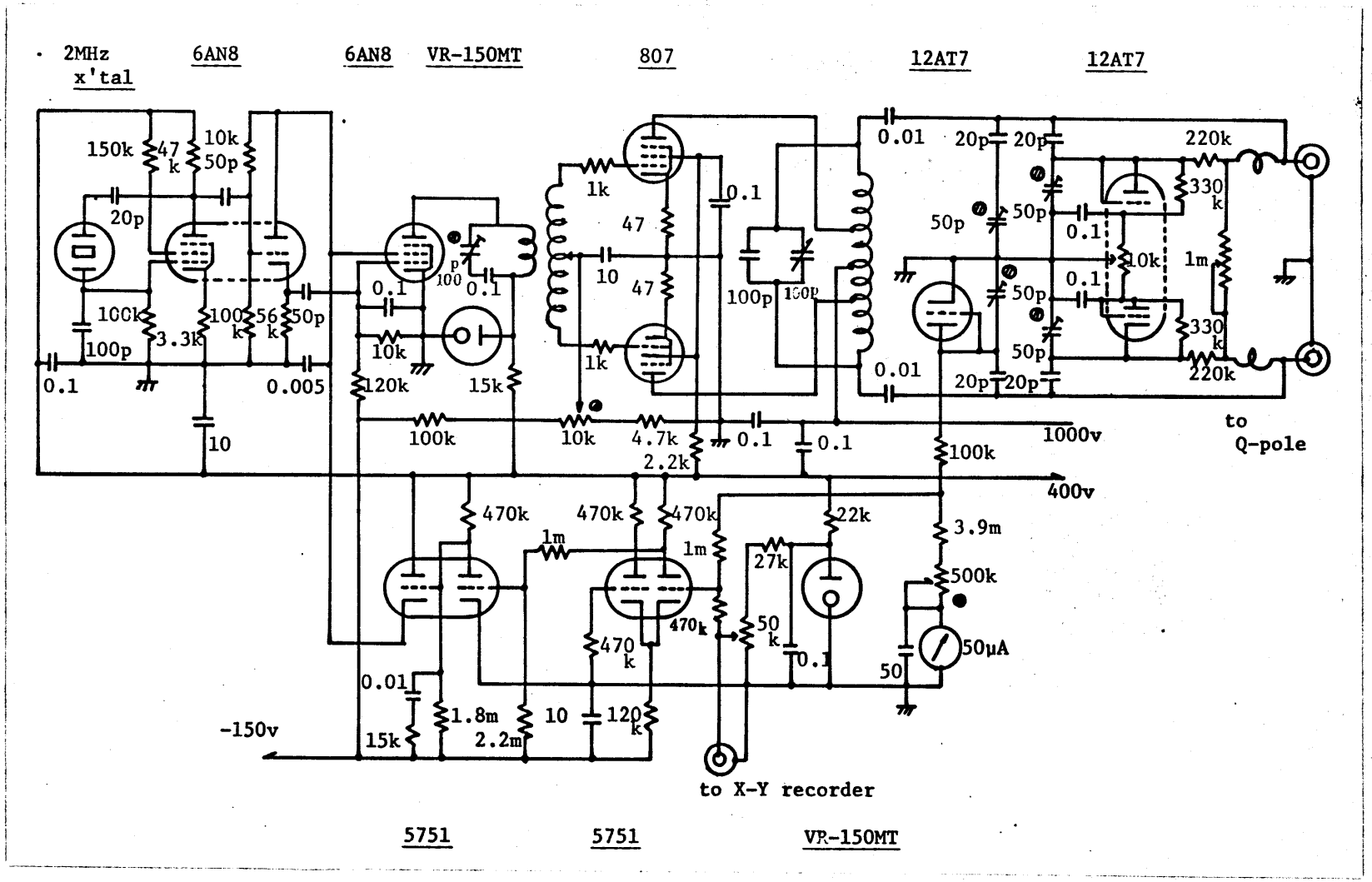

Fig. 4, Mass filter electronic circuit diagram for the AC/DC power generator.

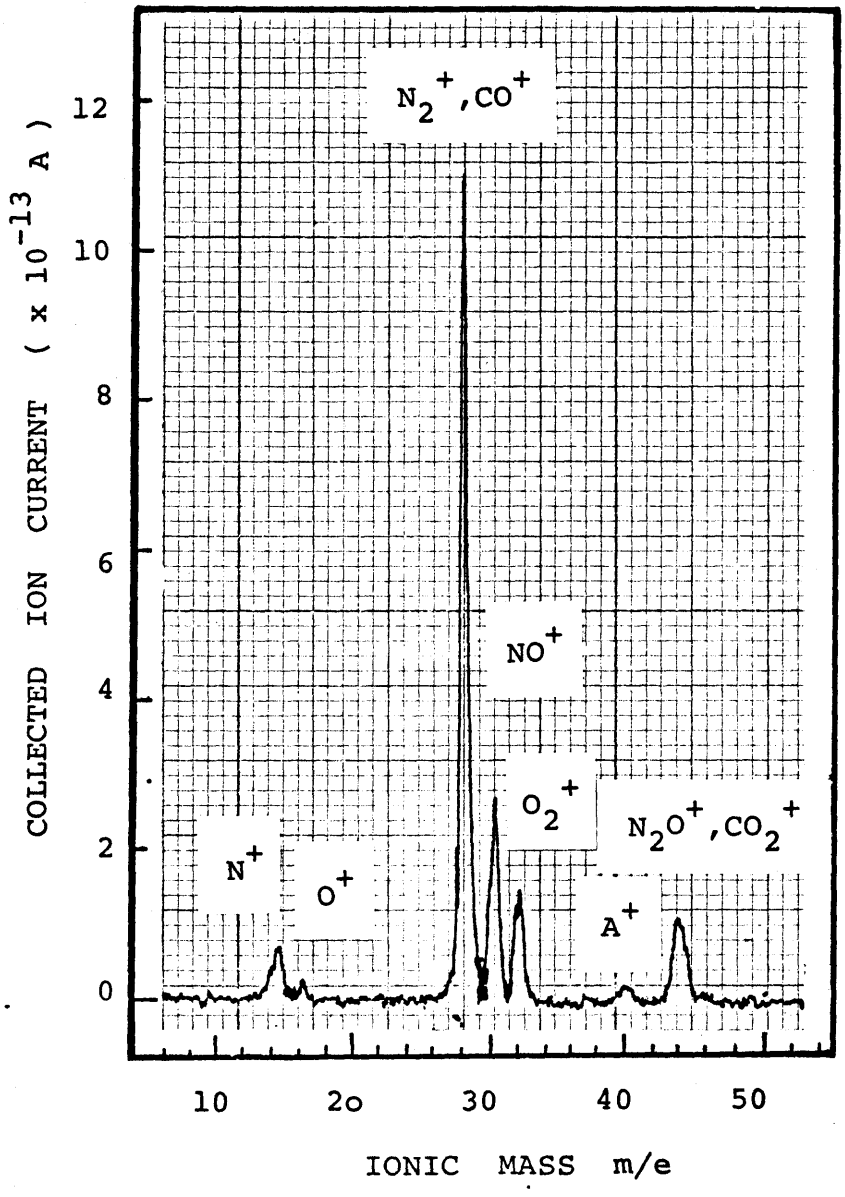

Fig. 5. Ionic mass scan in air discharge at pressure $P = 8 \times 10^{-5}$ torr. RF frequency f = 65 MHz. The mean ion beam energy $\bar{E}$ = 124 eV.

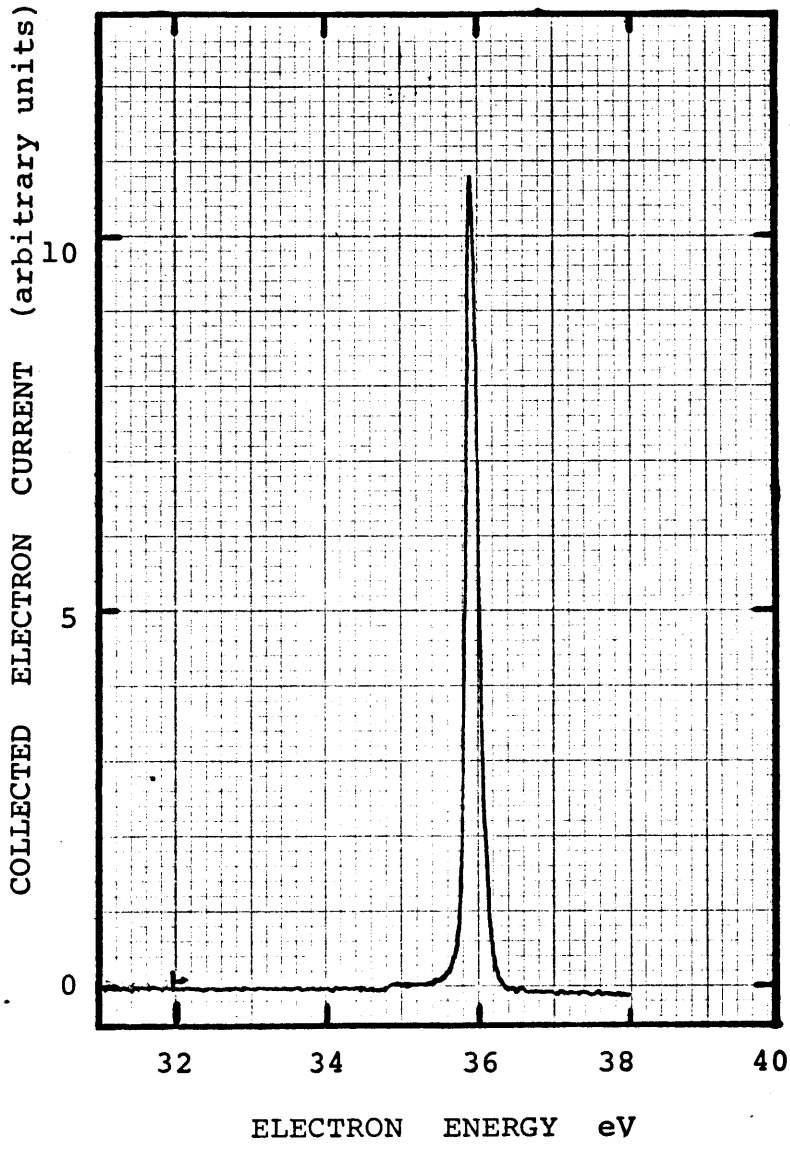

Fig. 6. Typical electron energy spectrum of electron gun.

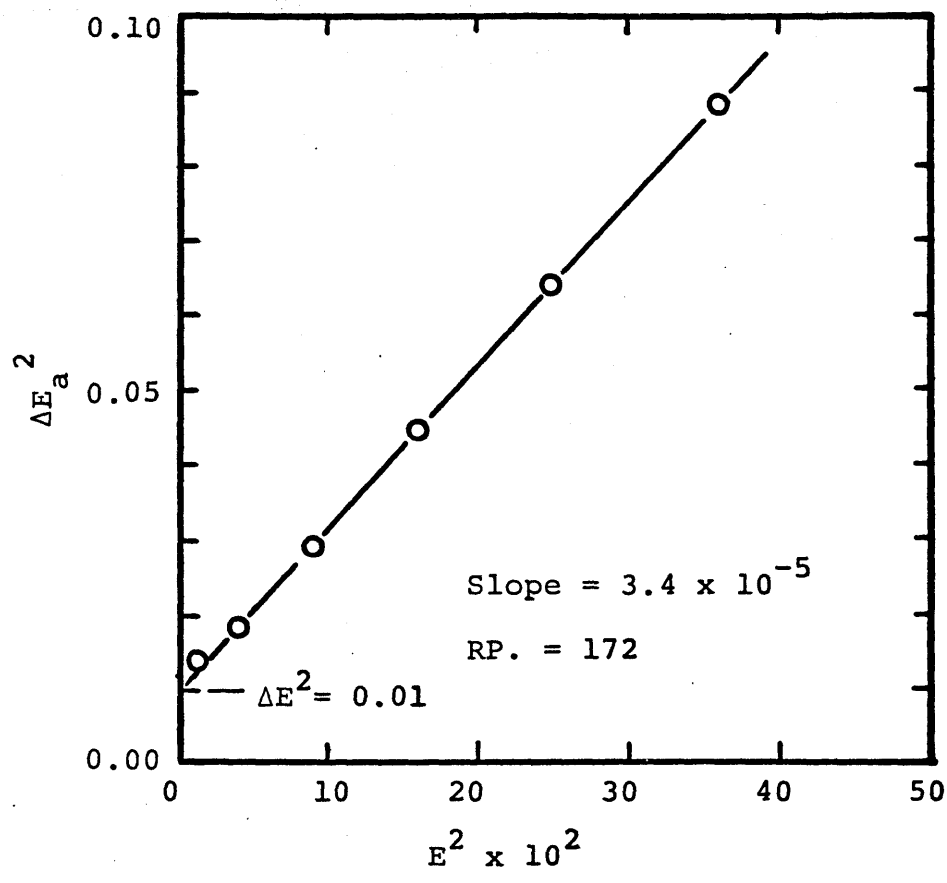

Fig. 7. Square of apparent energy half width ΔE_a vs. square of beam mean energy E^2. Intercept equals ΔE^2, the square of the actual energy half width; the slope is $(1/RP.)^2$, the reciprocal square of the energy analyzer resolving power.

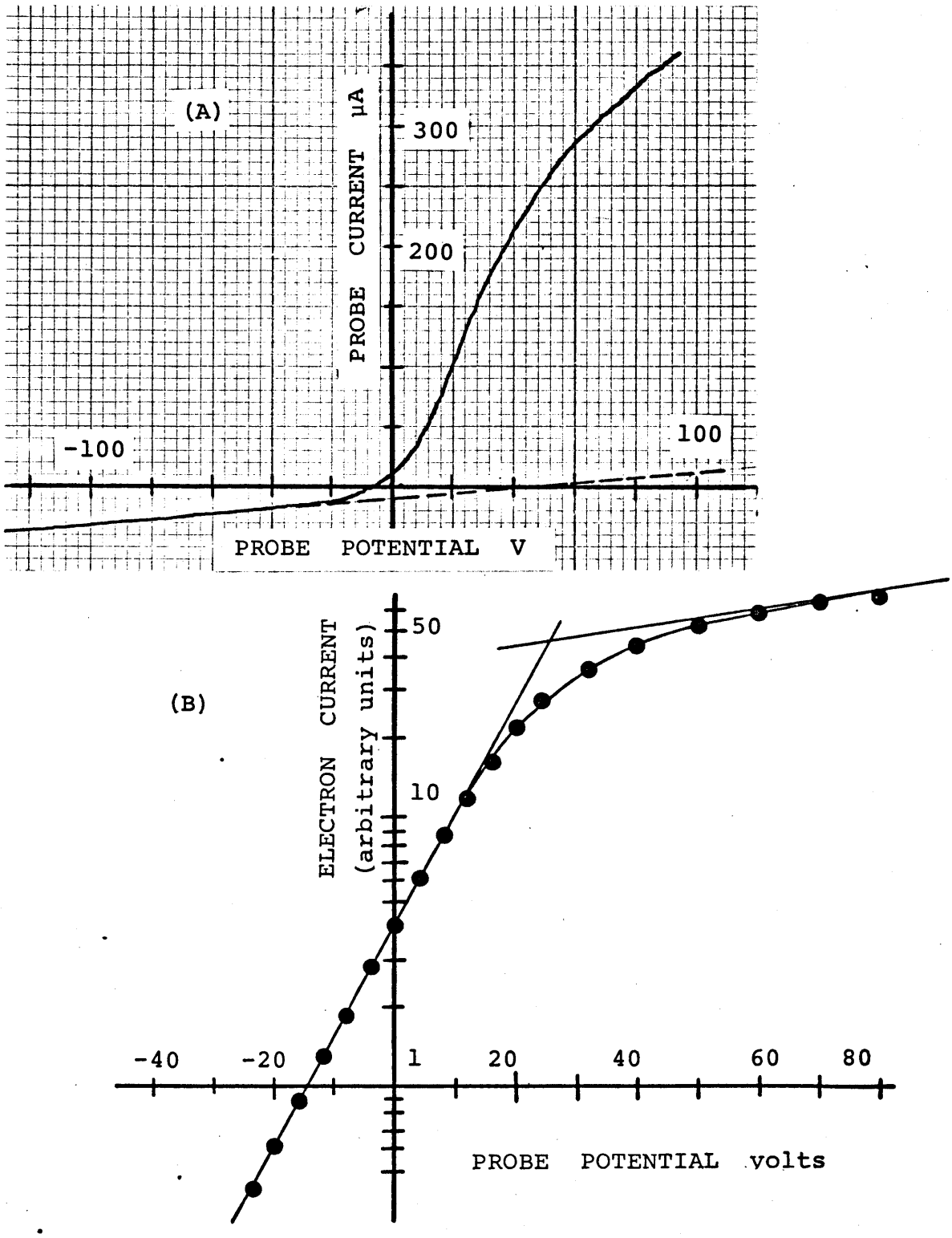

Fig. 8 . (A): Recorder tracing of a Langmuir probe measurement made near the axis of the plasma. (B): Determination of electron temperature from semilogarithimic plot of electron current vs. potential. The points are taken from (A).

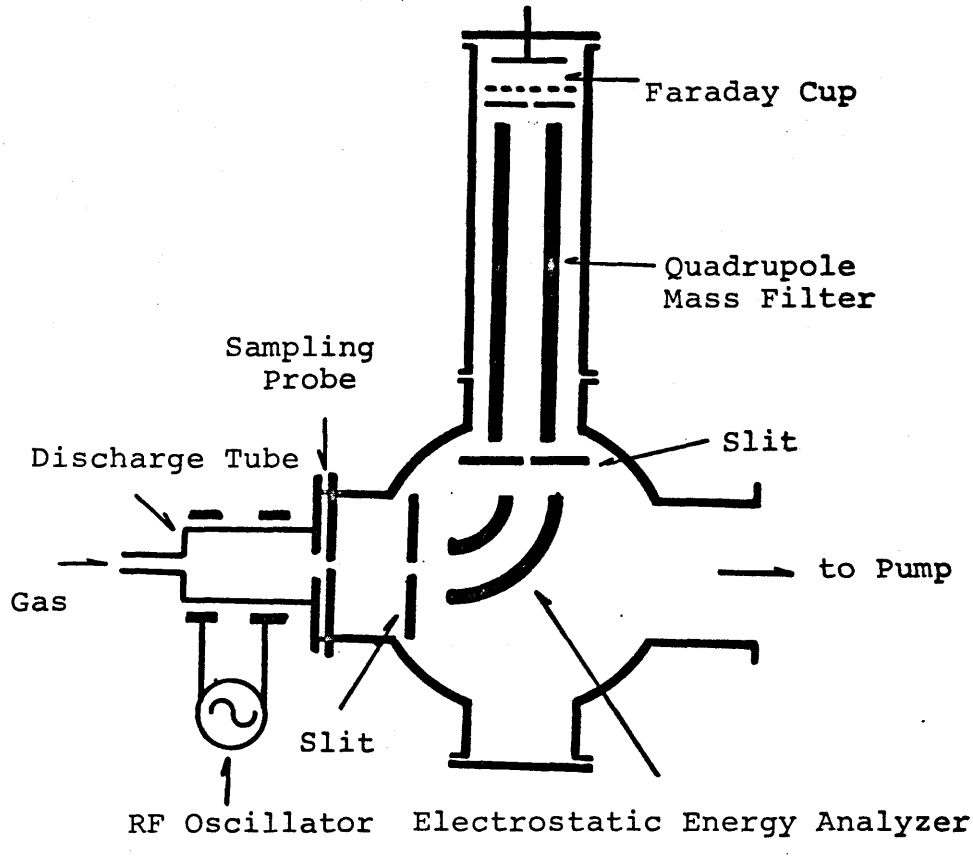

Fig. 9. Schematic diagram of experimental apparatus for studing energy dispersion of ions.

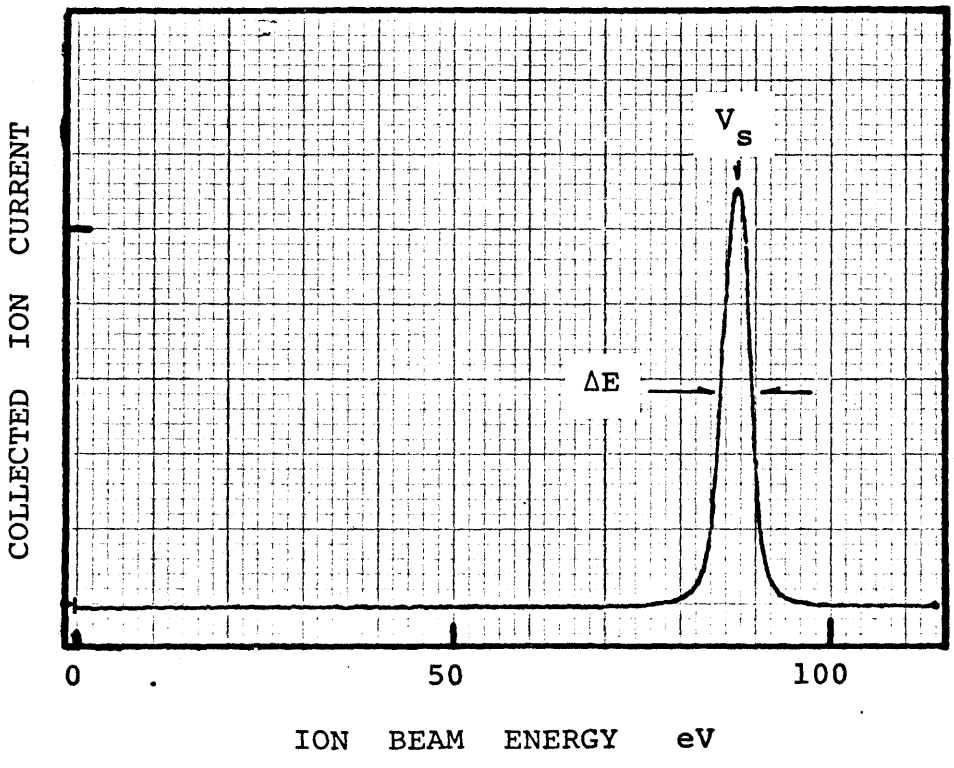

Fig. 10 . Typical energy distribution of the positive ion N_2^+, effused from an RF plasma. RF frequency f = 65 MHz, and its power W = 30 watts. Dischrge pressure P = 7×10^{-4} torr.

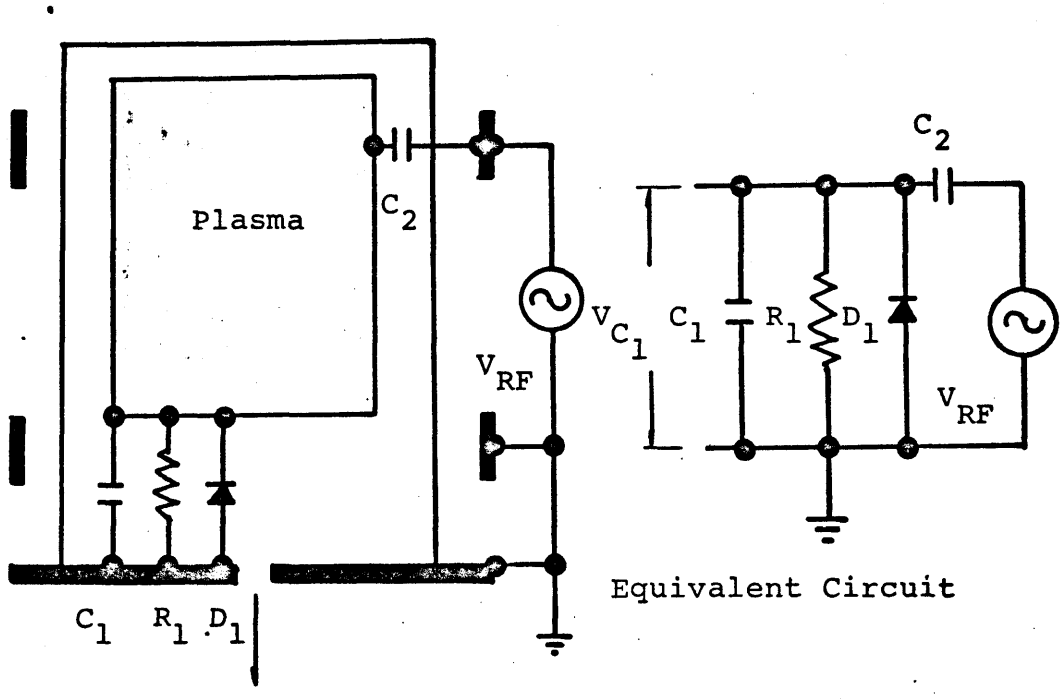

$$V_{C_1} = \frac{C_2}{C_1 + C_2} V_{RF} \simeq \frac{C_2}{C_1} V_{RF} \propto V_s$$

Fig. 11. Ion extraction model for plasma-sheath system and its equivalent circuit.

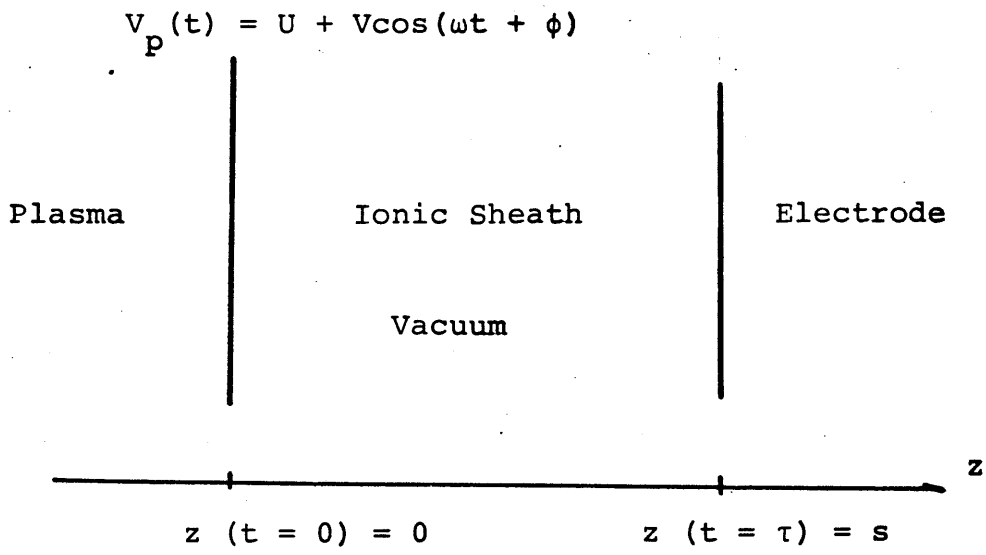

Fig. 12. Illustrating co-ordinate system.

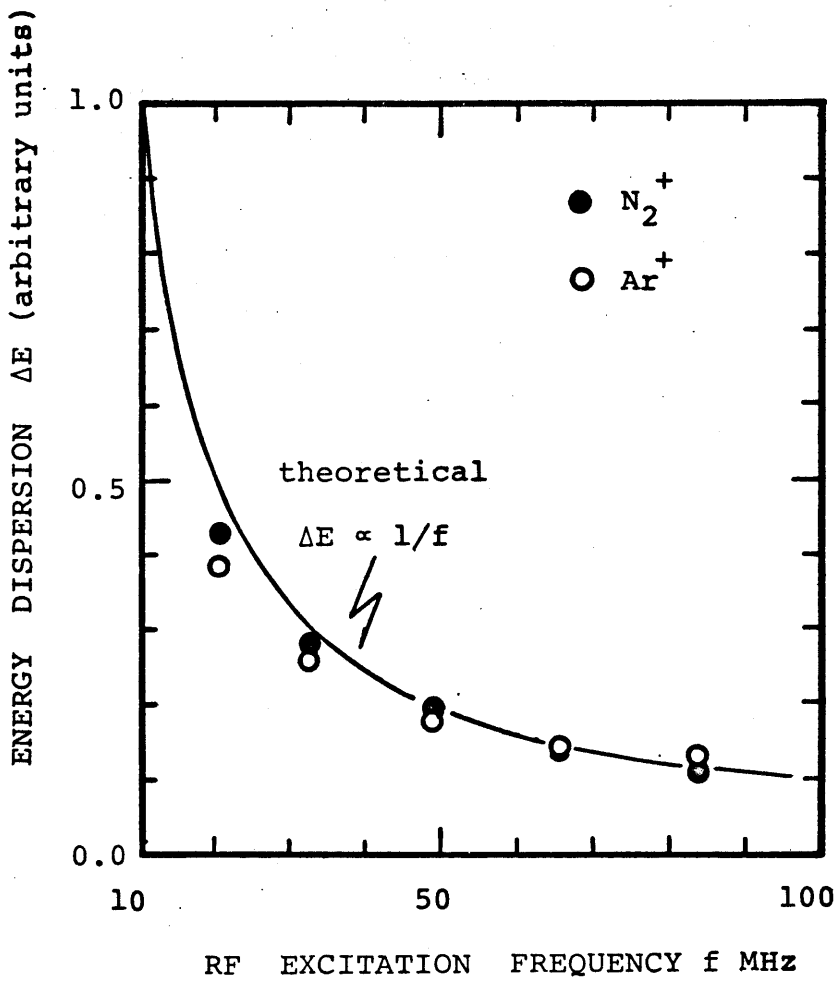

Fig. 13. Dependence of the energy dispersion ΔE on RF excitation frequency f. The mean ion beam energy $\bar{E}$ is 102 eV.
Normalized to unity at f = 10 MHz.

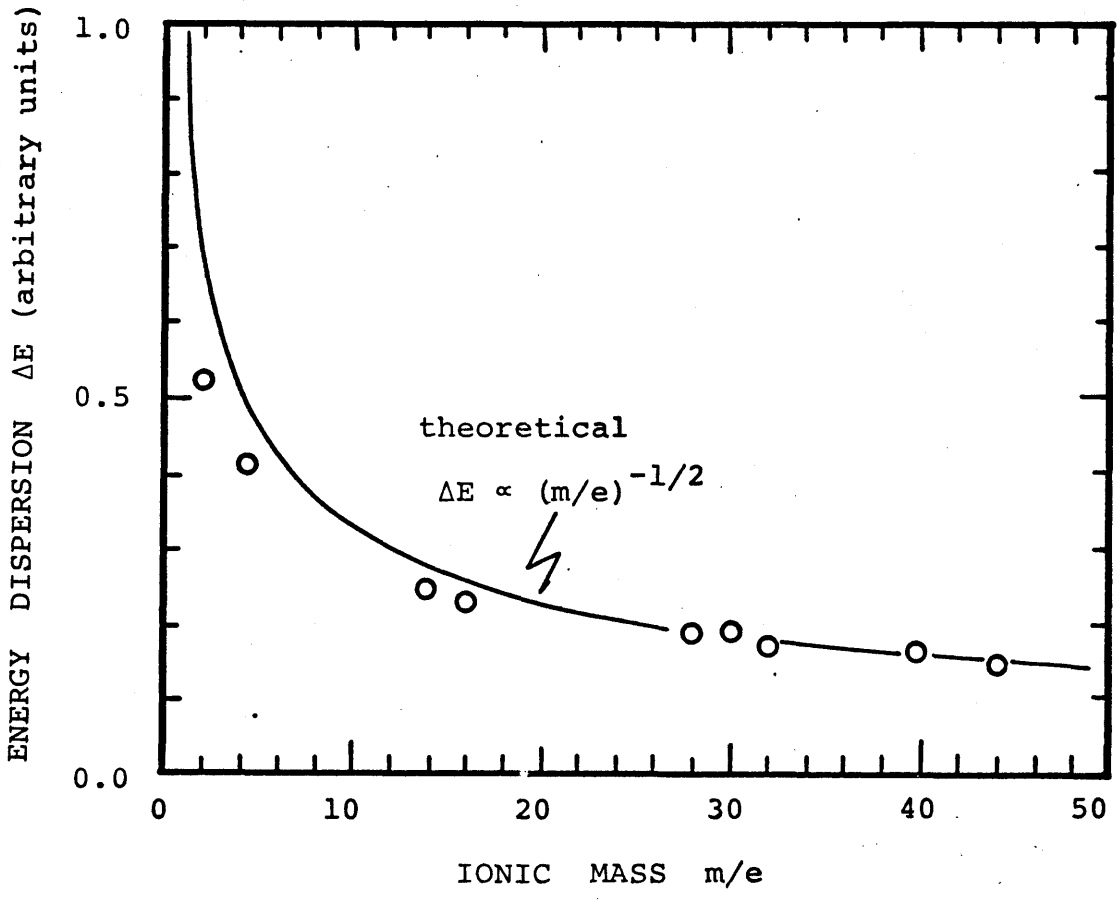

Fig. 14. Dependence of the energy dispersion ΔE on ionic mass m/e. The mean beam energy $\bar{E}$ is 124 eV. RF frequency f is 65 MHz and its power is 40 watts. Normalized to unity at m/e = 1.

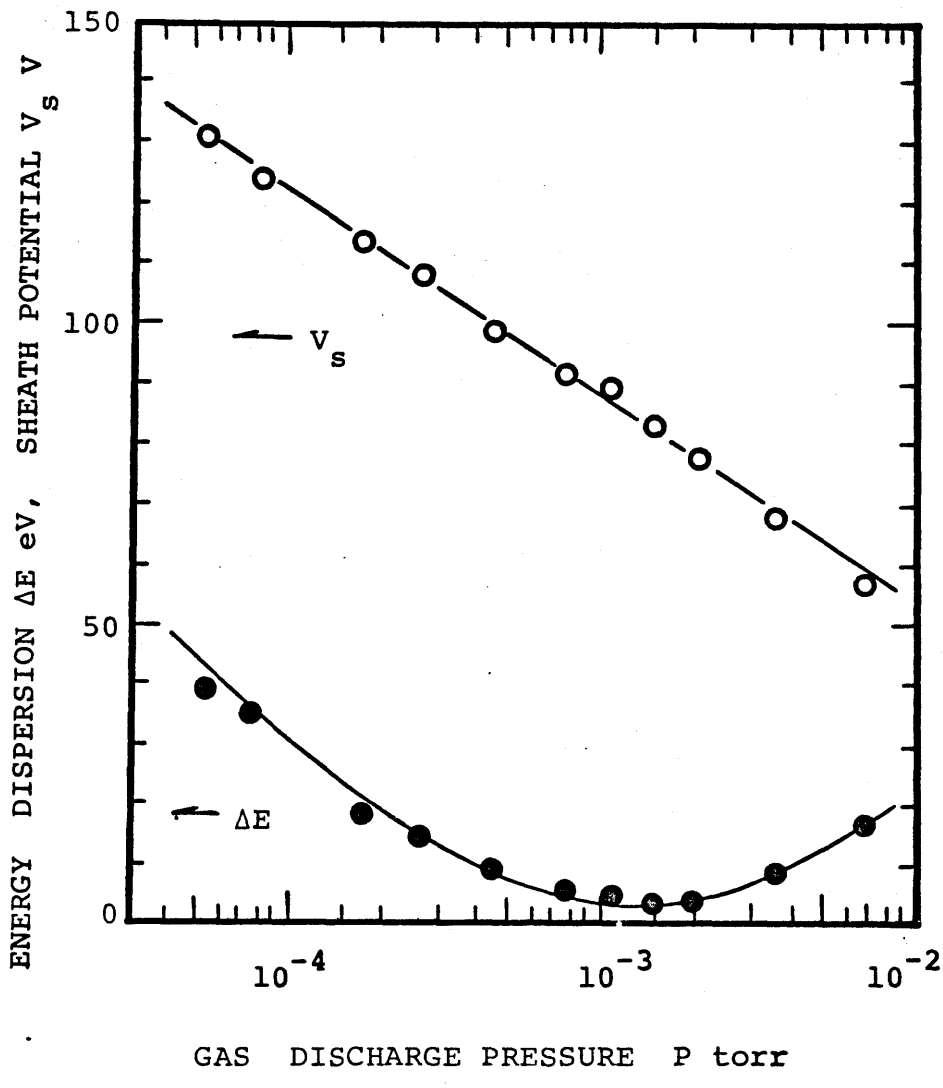

Fig. 15. Dependence of the energy dispersion ΔE and the exess energy eV_s, when the discharge pressure P is varied. f = 65 MHz, W = 40 watts, and ionic mass m/e = 28.

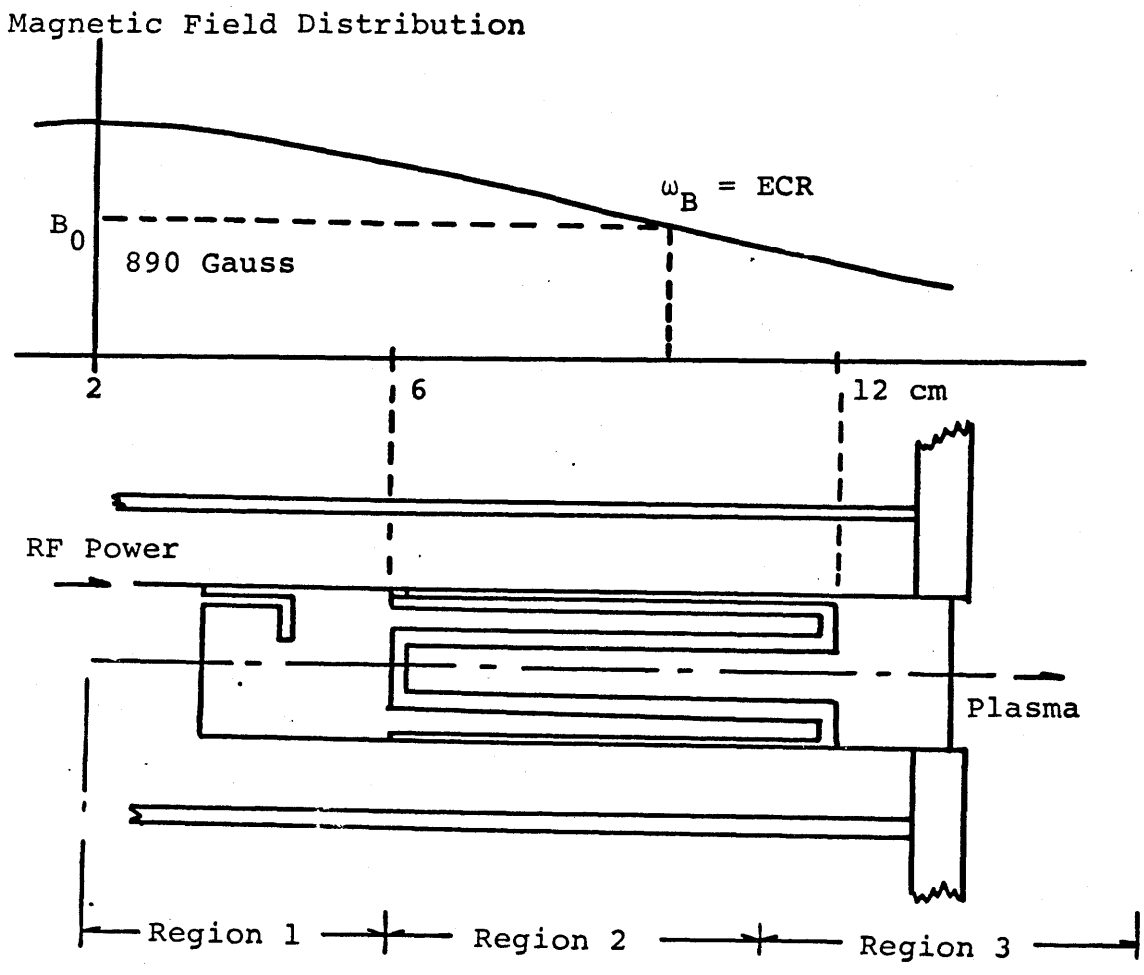

Fig. 16 . RF coupling device (Lisitano coil) and axial magnetic field distribution.

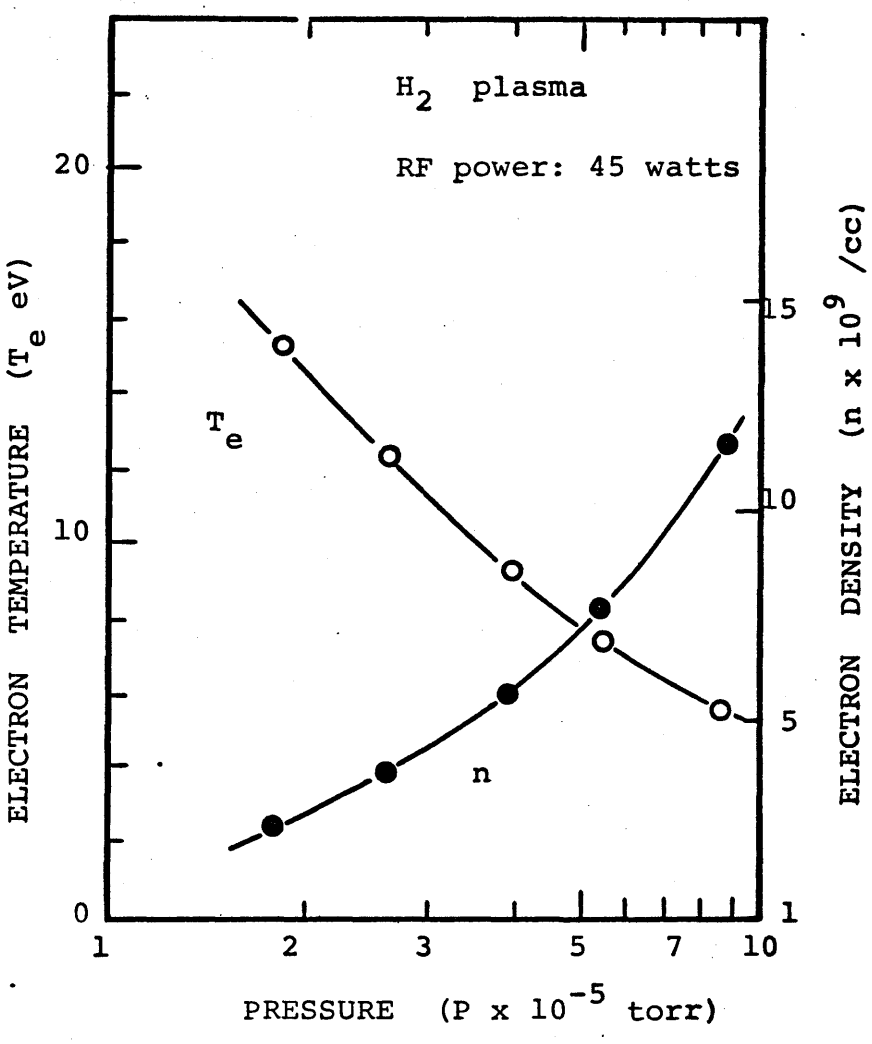

Fig. 17. Electron temperature and electron density on the plasma column vs. pressure.

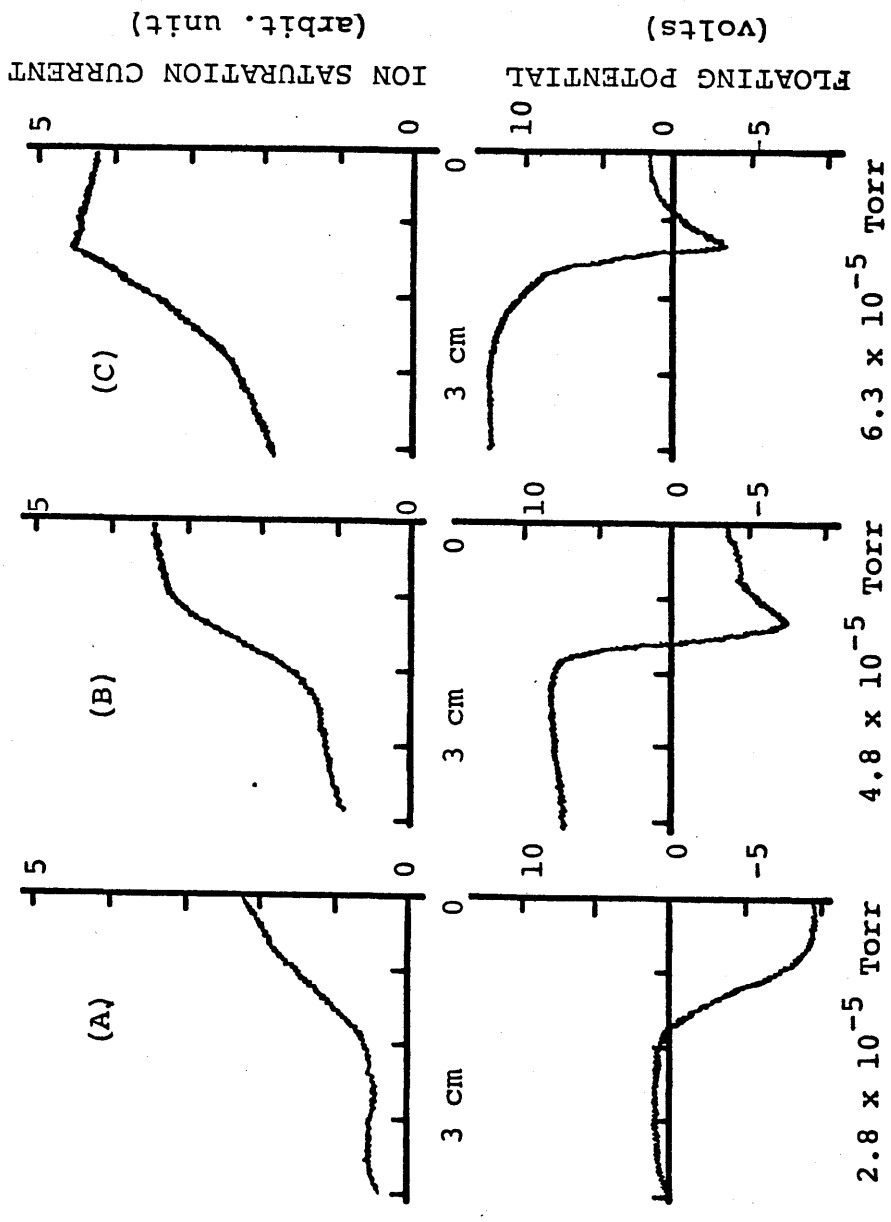

Fig. 18. Radial distributions of ion saturation current, and floating potential as a parameter of pressure.

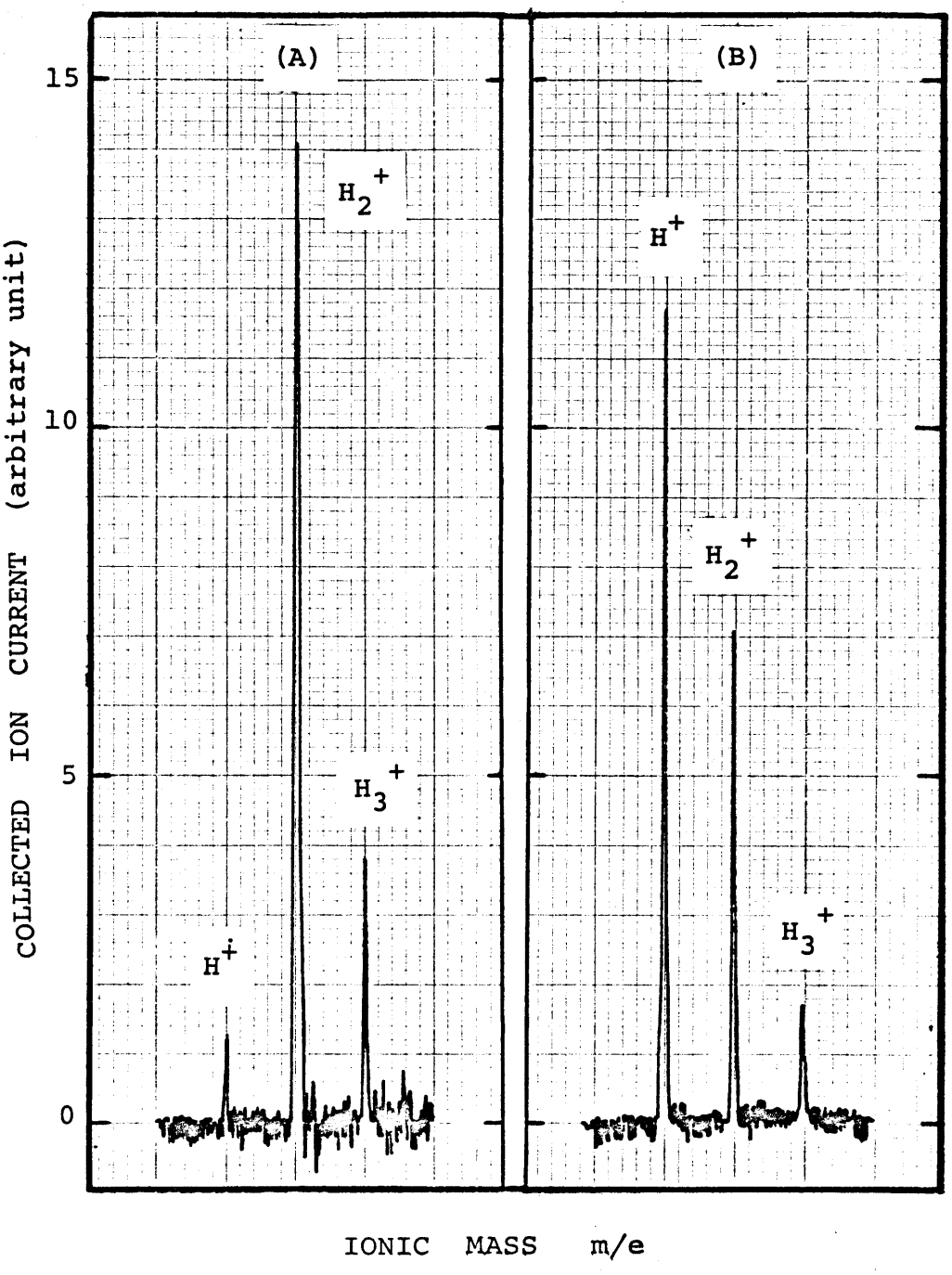

Fig. 19. Effect of the electron temperature on the mass spectrum of the resulting ions. (A): 7.1 eV and (B): 10.3 eV. Mean beam energy is 200 eV.

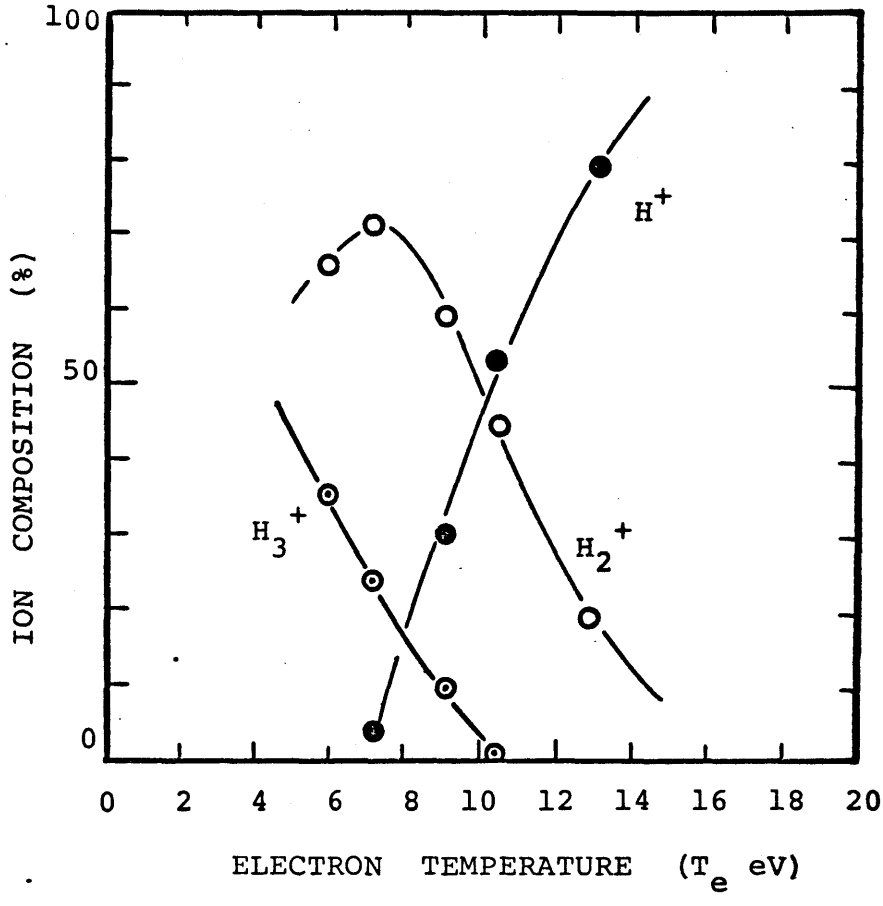

Fig. 20. Dependence of proportions of various ions on electron temperature.

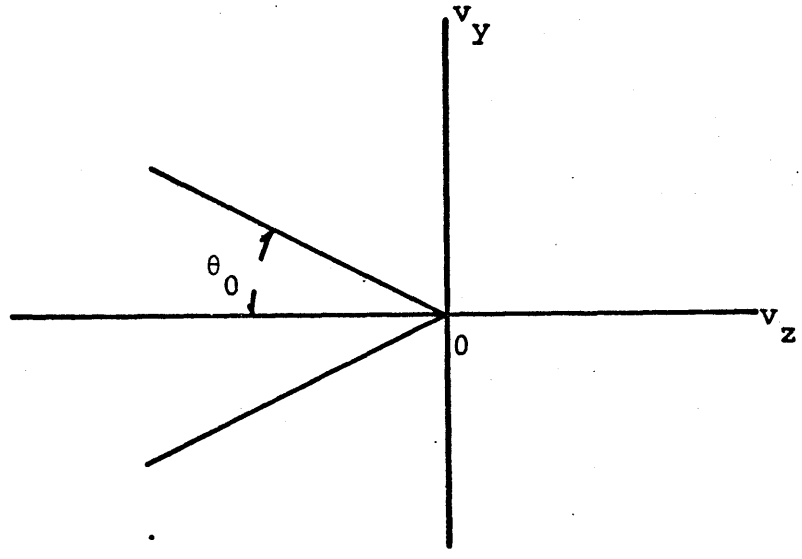

Fig. 21. Schematic drawing of velocity space with particles confined to escape cone of half-angle θ_0.

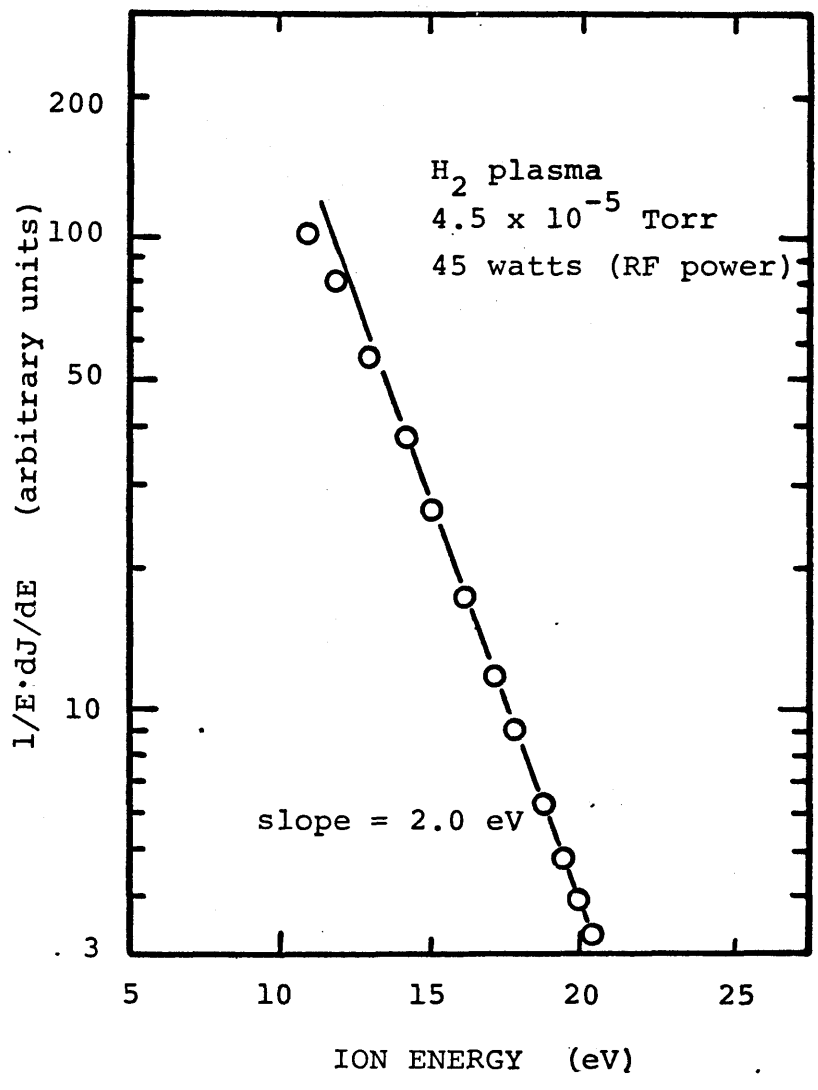

Fig. 22 . Logarithm plot of the energy distribution of ion flux as a function of ion energy.

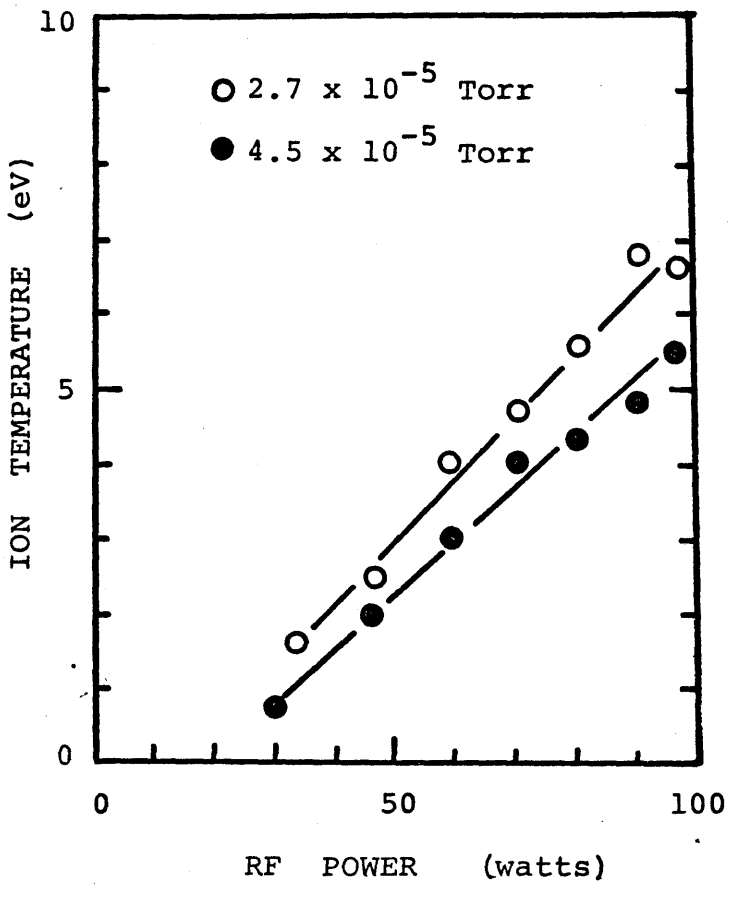

Fig. 23. Ion temperature vs. RF power as a parameter of pressure (H_2).

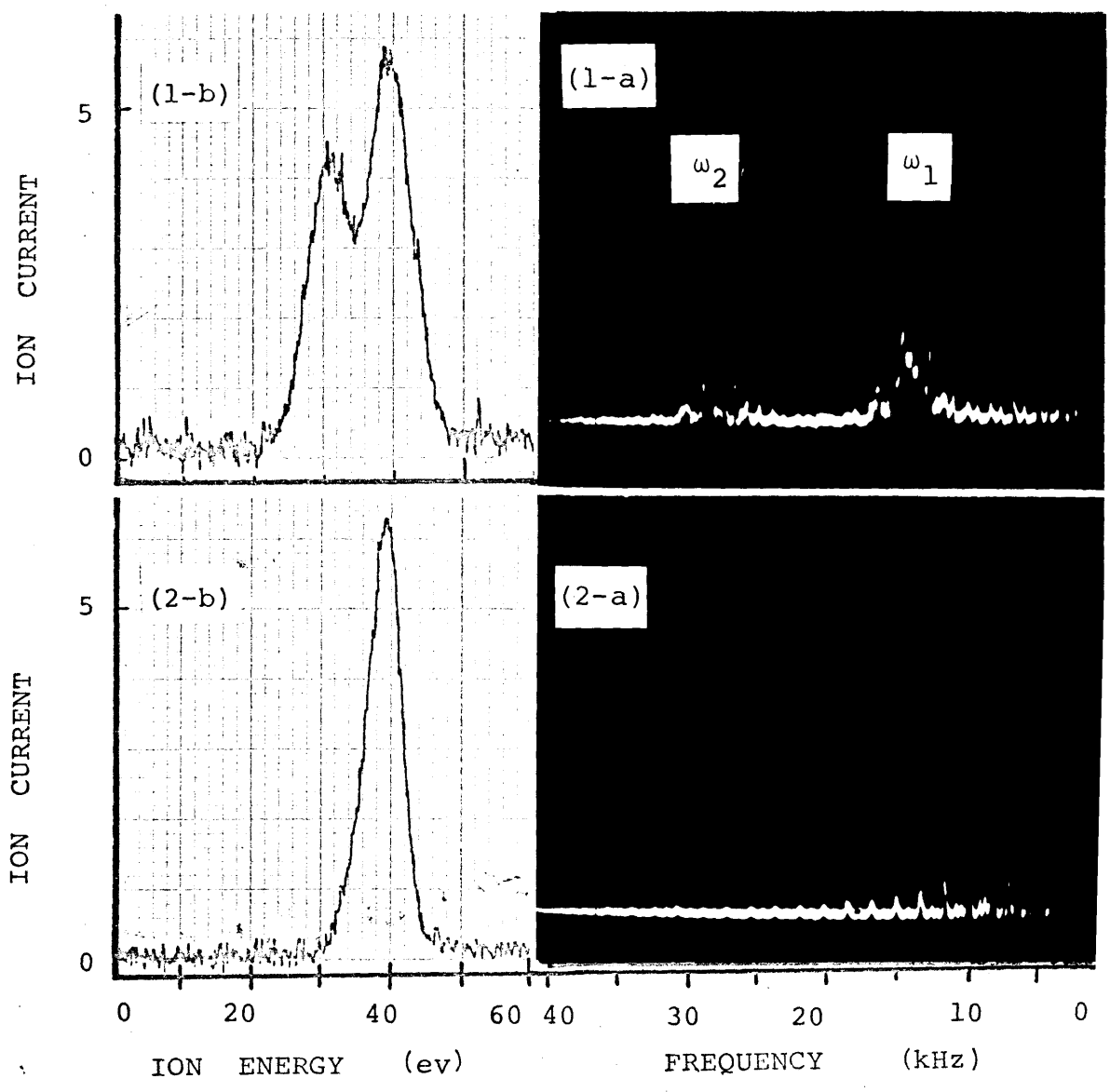

Fig. 24. Relations between (a): the frequency spectra and (b): the profile of ionic energy distribution functions. (1): Unstable, (2): Stable.

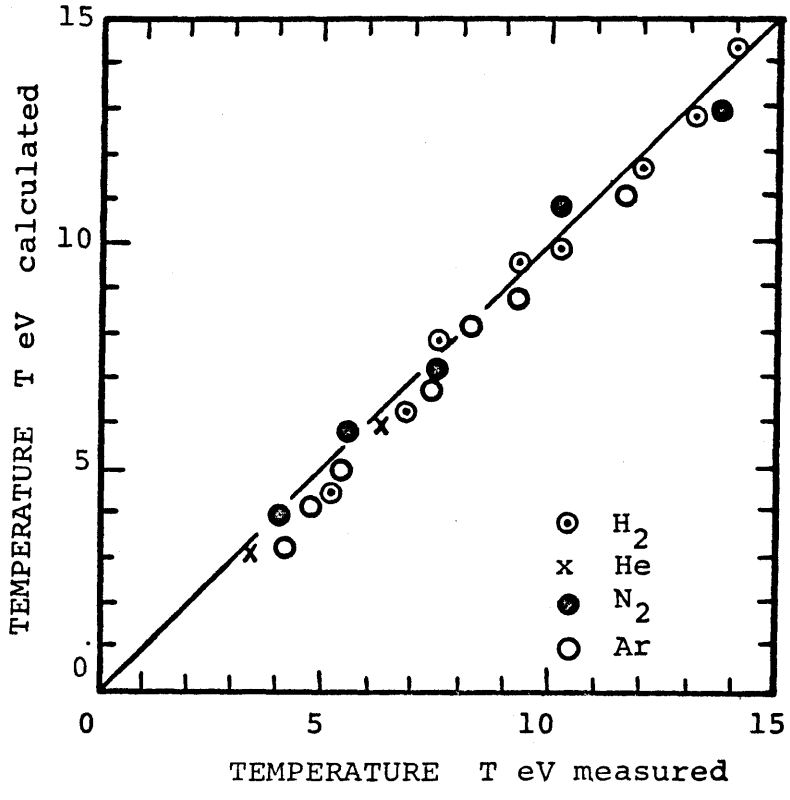

Fig. 25. Comparison of calculated- and experimental-temperature.

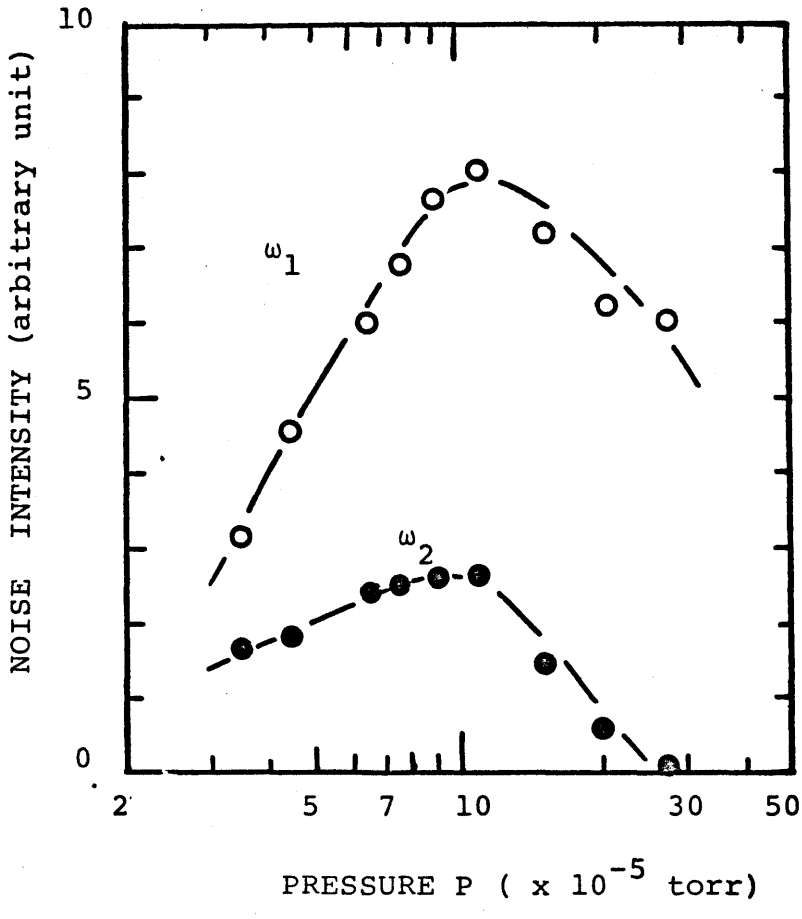

Fig. 26. Ion acoustic wave amplitude vs. pressure. RF power is 30 watts.

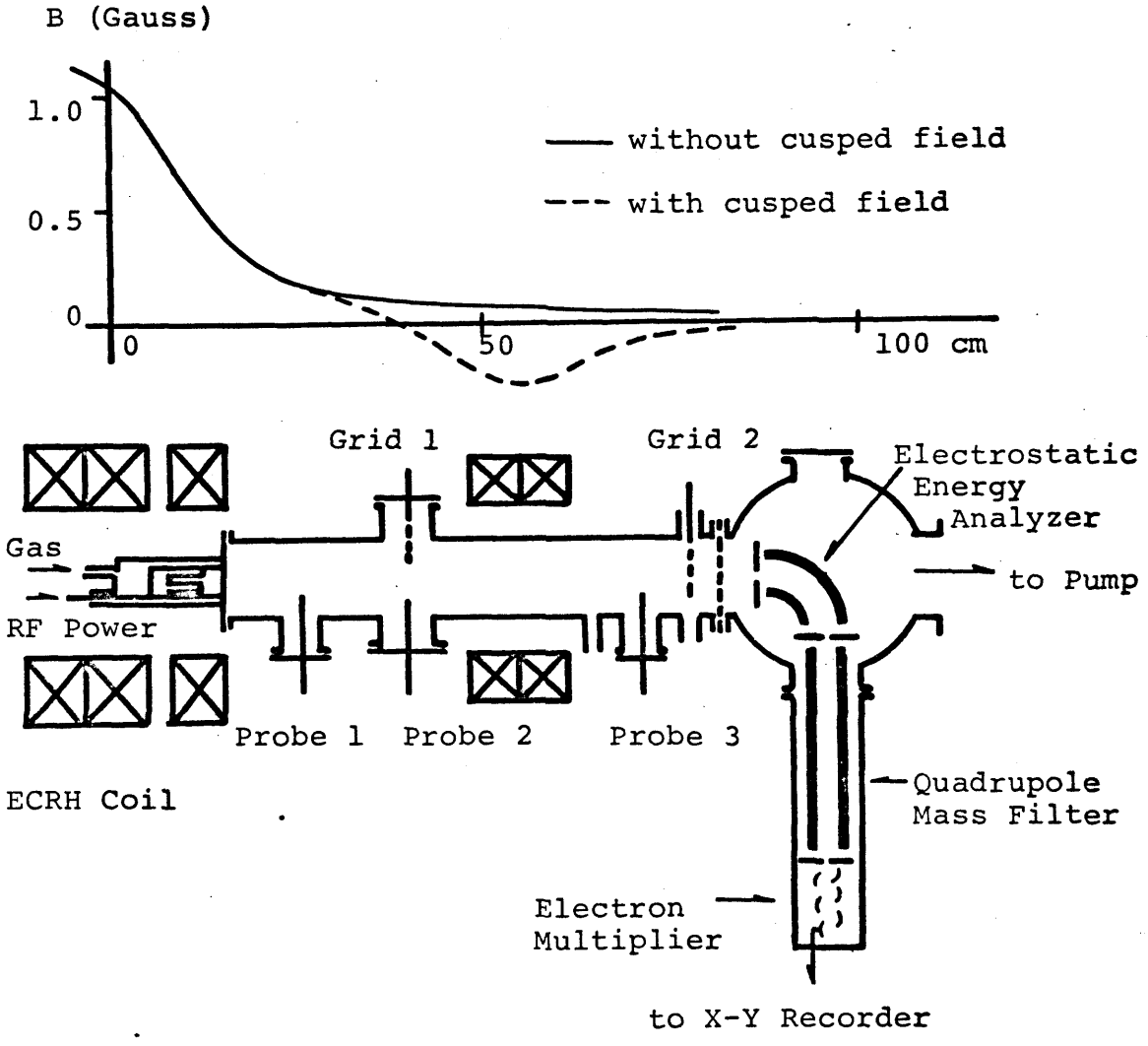

Fig. 27. Schematic diagram (bottom) and magnetic field distribution along the system (top).

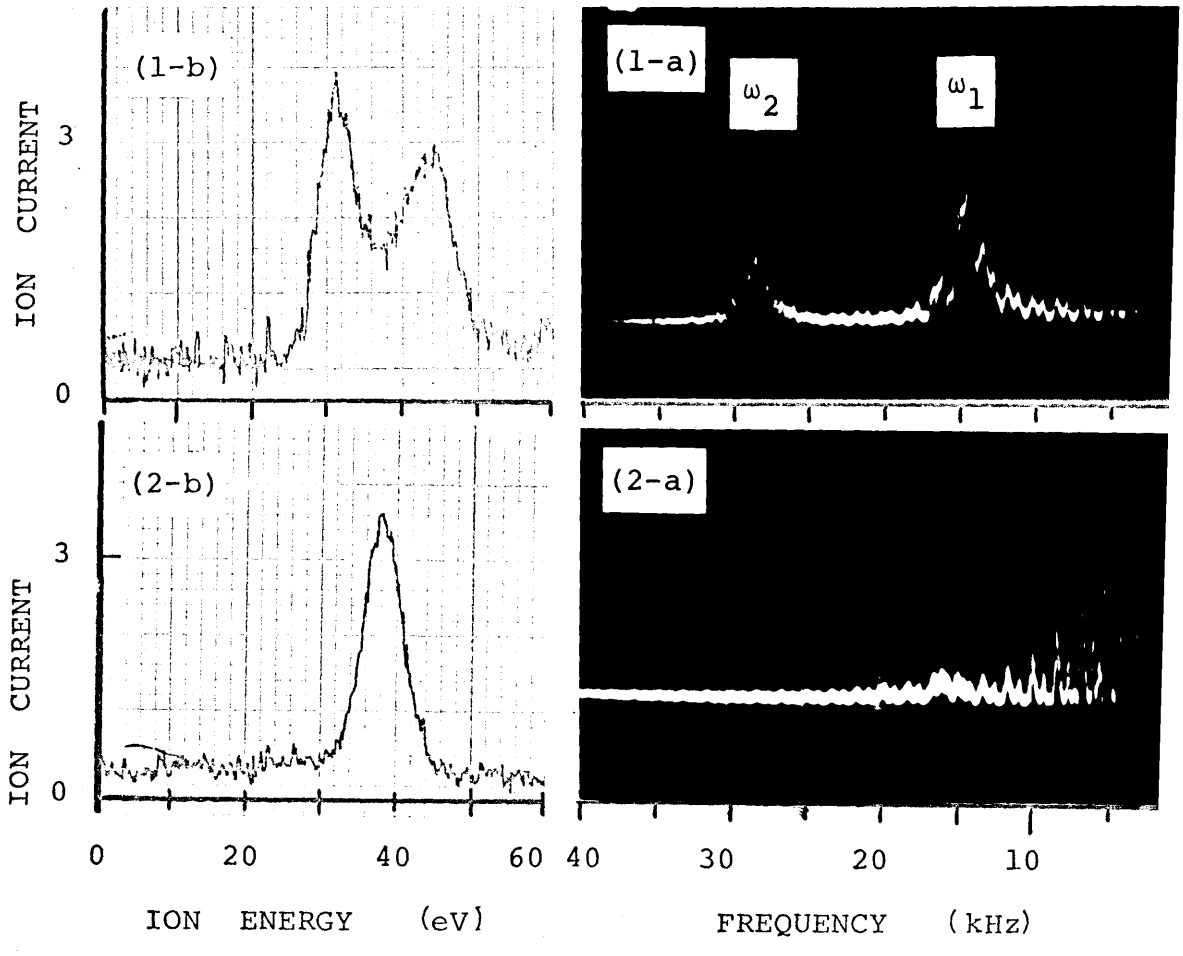

Fig. 28. Relations between (a): the frequency spectra and (b): the profile of ionic energy distribution functions. (1): without cusped-field and (2): with cusped-field.

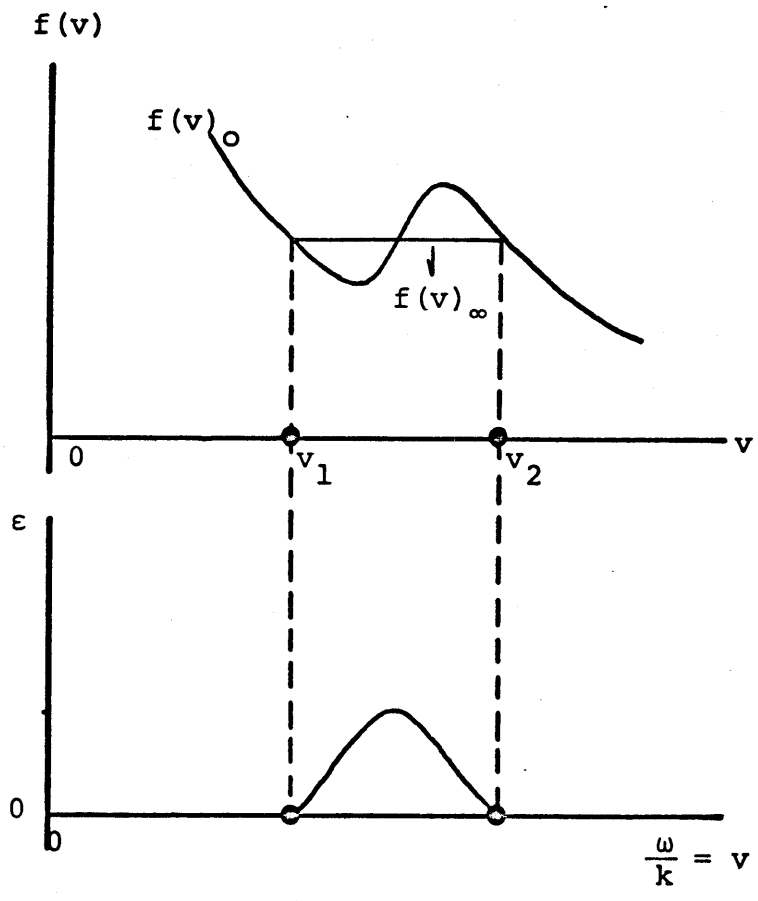

Fig. 29 . Ionic energy distribution function with double-hump (top) and its spectral density distribution (bottom).

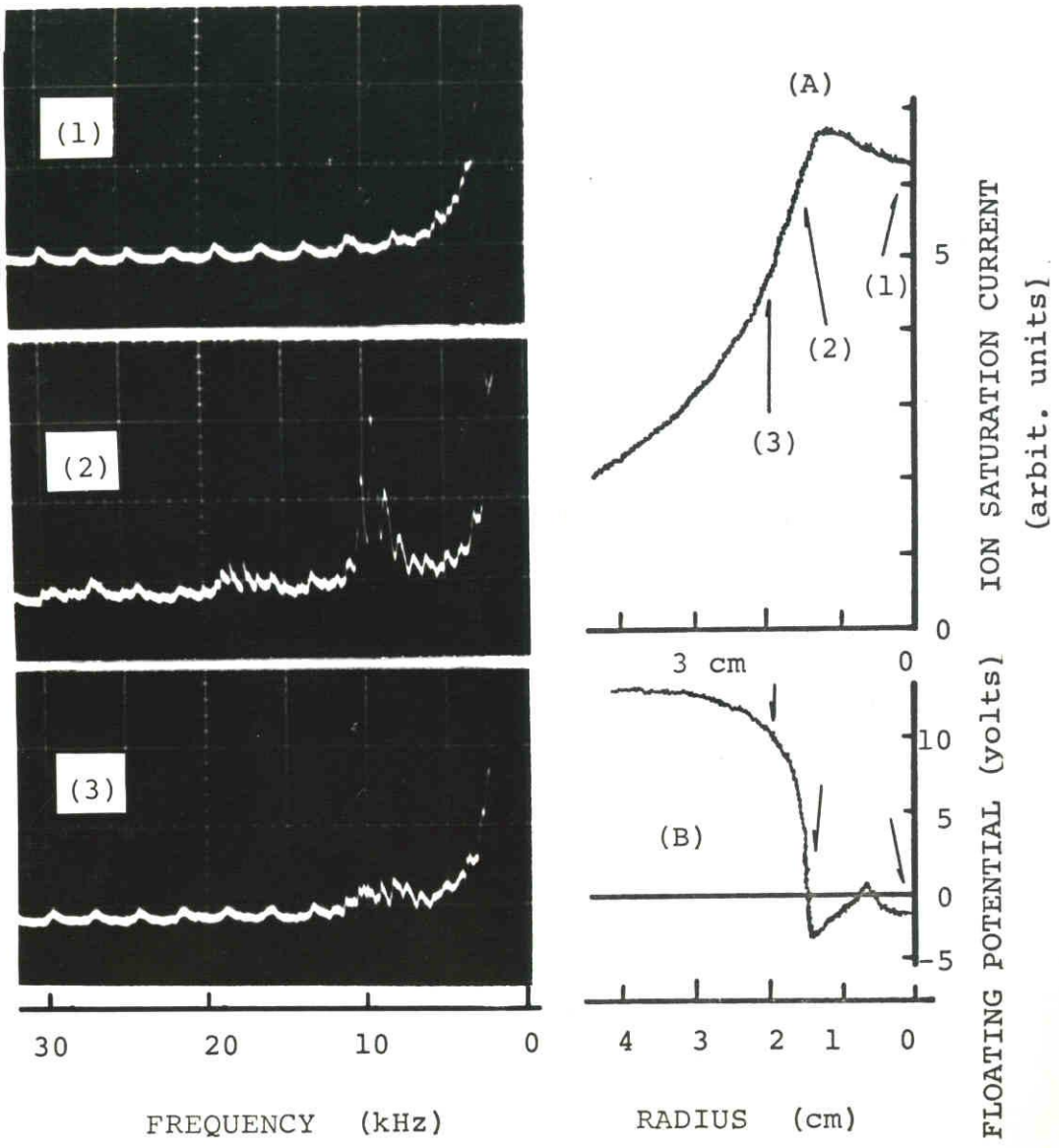

Fig. 30. Radial distributions of ion saturation current, floating potential, and typical output from the spectrum-analyzer.

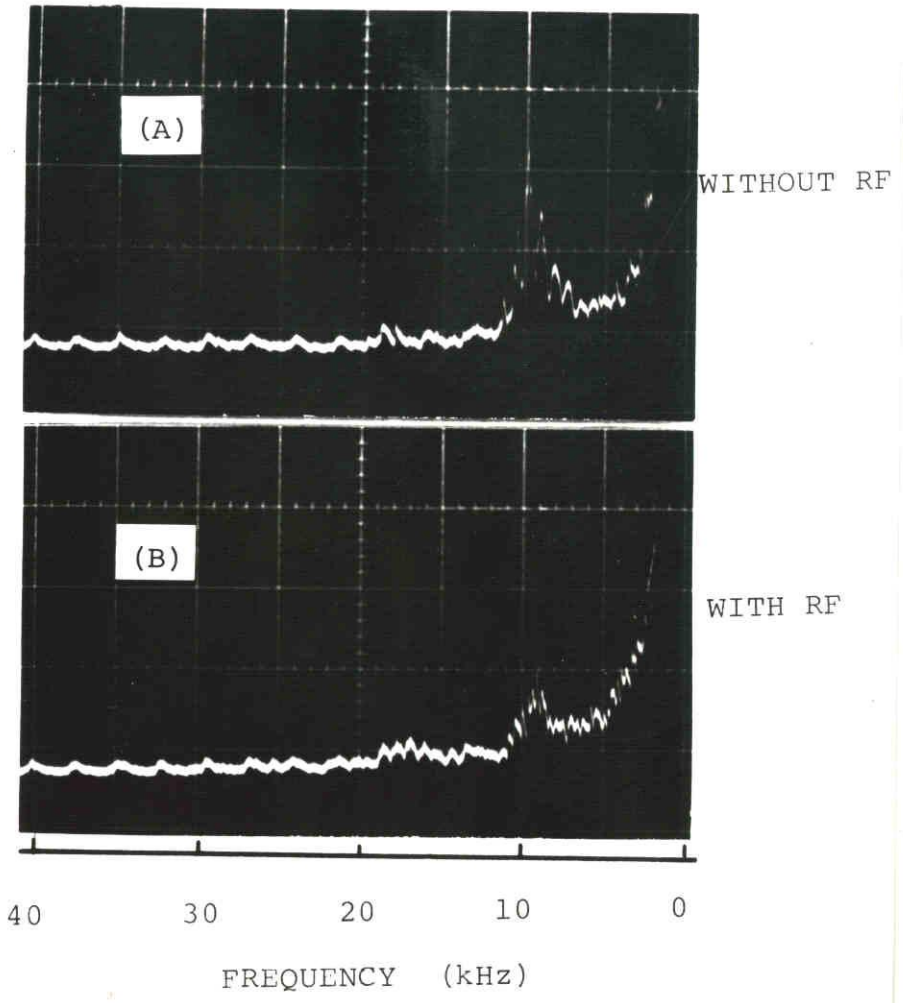

Fig. 31. Spectrum-analyzer output showing the instability at 10 kHz for (A) without RF field and (B) with optimum RF field. RF voltage is 12 volts peak to peak and the frequency is 10.3 kHz.

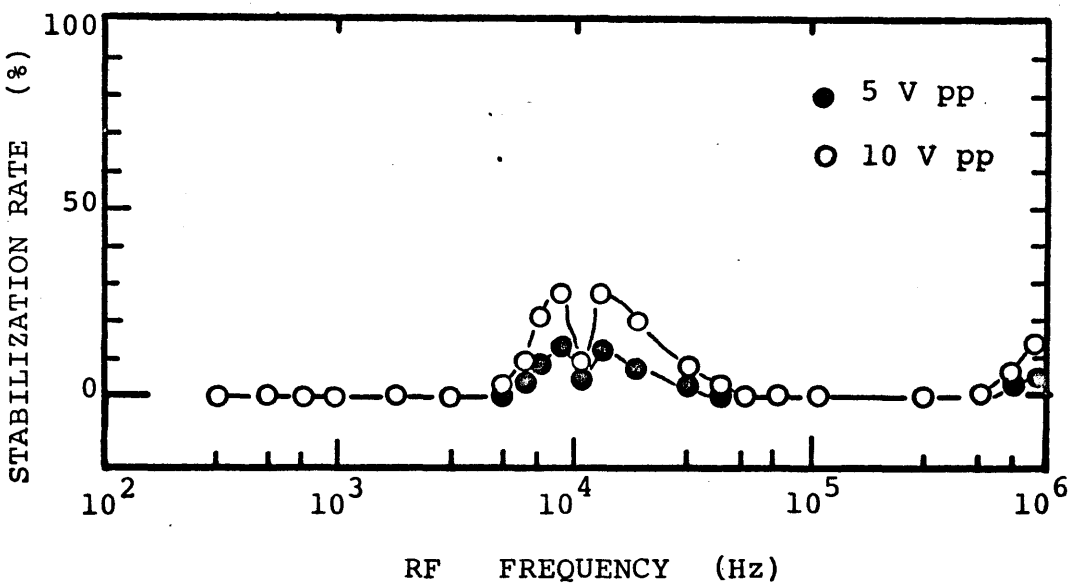

Fig. 32. Stabilization rate versus RF field frequency as a parameter of RF voltage.

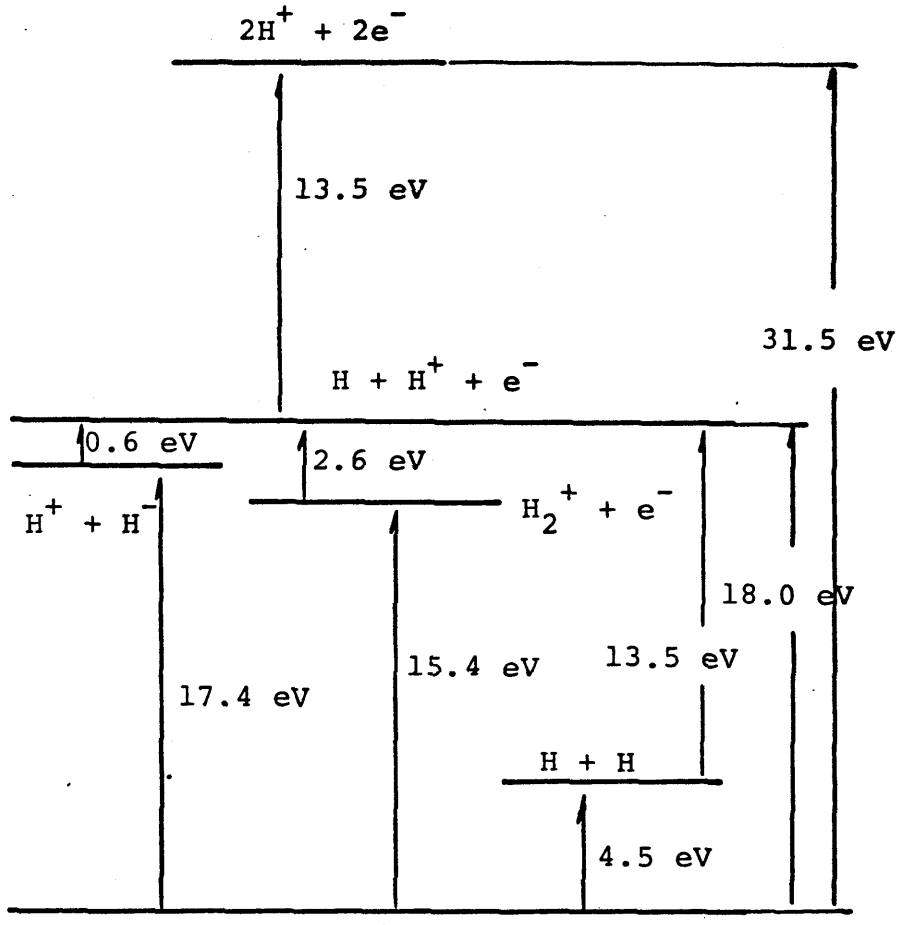

Fig. 33. Dissociation levels of the hydrogen molecule.

Publications by Y. Okamoto

1). Electronic Recording Fluxmeter: S. Usami, A. Miyahara, K. Matsuura, and Y. Okamoto: Tech. Rep. Inst. Plasma Phys. Nagoya Univ. IPPJ-DT-7 (1964).

2). Measurements of BSG Plasma with a 2 mm Microwave Interferometer (BSG-4): J. Fujita, Y. Okamoto, K. Miyamoto, S. Kawasaki, N. Inoue, Y. Suzuki, K. Adachi, and T. Uchida: Kakuyugo-Kenkyu, 17 (1966) 540.

3). Electronics Data Book (circuit): Edited by Electronics Shop Inst. Plasma Phys. Nagoya Univ. Tech. Rep. Inst. Plasma Phys. Nagoya Univ. IPPJ-DT-11 (1967).

4). 2 mm Microwave Interferometer Measurements of the Determination of Plasma Parameters in Controlled Fusion Experiment of BSG I Device: Y. Miyoshi, Y. Okamoto, T. Uchida, and J. Fujita: Bulletin Nagoya Inst. Tech., 19 (1967) 269.

5). Investigation of Plasma Expansion in a Uniform Field and Shock Formation due to a Magnetic Barrier: Y. Miyoshi and Y. Okamoto: Japan J. appl. Phys., 7 (1968) 927.

6). Comparison of 35 GHz Microwave Reflection Probe Method with 150 GHz Microwave Interferometry: Y. Okamoto and J. Fujita: Japan J. appl. Phys., 8 (1969) 281.

7). Energy Distribution of Positive Ions Extracted from an RF Plasma: Y. Okamoto and H. Tamagawa: J. Phys. Soc. Japan, 27 (1969) 270.

8). RF Ion Source: Y. Okamoto and H. Tamagawa: Oyo-Butsuri, 38 (1969) 1114.

9). Dependence of Energy Dispersion on Ion Mass Effused from an RF Plasma: Y. Okamoto and H. Tamagawa: J. Phys. Soc. Japan, 28 (1970) 269.

10). Energy Dispersion of Positive Ions Effused from an RF Plasma: Y. Okamoto and H. Tamagawa: Res. Rep. Inst. Plasma Phys. Nagoya Univ. IPPJ-87 (1970).

11). Quadrupole Mass Filter and its Application to the Study of Plasma: Y. Okamoto and H. Tamagawa: Tech. Rep. Inst. Plasma Phys. Nagoya Univ. IPPJ-T-5 (1970).

12). Energy dispersion of Positive Ions Effused from an RF Plasma: Y. Okamoto and H. Tamagawa: J. Phys. Soc. Japan, 29 (1970) 187.

13). Self-excited Ion Acoustic Waves Generated by Means of Electron Cyclotron Resonance and its Stabilization: Y. Okamoto and H. Tamagawa: Phys. Lett., 32A (1970) 279.

14). Excitation and Stabilization of Ion Acoustic Waves inan RF Plasma: Y. Okamoto and H. Tamagawa: Plasma Phys., 13 (1971) 71.

15). Microwave Discharge Ion Source for Chemical Accelerator: Y. Okamoto and H. Tamagawa: Japan J. appl. Phys., 10 (1971) 165.

16). Chemical Reactions in an RF Plasma: Y. Okamoto and H. Tamagawa: to be submitted in Japan J. appl. Phys., (1971).

17). Stabilization of Drift Instabilities in an RF Plasma: Y. Okamoto and H. Tamagawa: to be submitted in Plasma Phys., (1971).